Simulation of ionic transition-metal crystals: The cluster model and the cluster-lattice interaction in the light of the theory of electronic separability

Víctor Luaña
Departamento de Matemáticas y Departamento de Química Física y Analítica, Facultad de Química, Universidad de Oviedo, E-33007 Oviedo, Spain

L. Pueyo
Departamento de Química Física y Analítica, Facultad de Química, Universidad de Oviedo, E-33007 Oviedo, Spain
(Received 31 August 1988)

The cluster model often applied to the study of transition-metal ions in ionic crystals is rigorously formulated in the framework of the theory of electronic separability (TES). This theory shows that the cluster-lattice coupling appearing in the effective cluster Hamiltonian should include two separate operators: (1) the lattice effective potential containing nuclear attraction, Coulomb, and exchange terms, and (2) a lattice projection operator enforcing the cluster-lattice orthogonality required by the Pauli principle. The analysis of the TES equations also suggests a hierarchy of lattice models for dealing with the cluster-lattice interaction in an approximate way. Using a Hartree-Fock-Roothaan description for the intracluster interactions, three of these models are investigated and illustrated by means of several examples. First, the familiar point-charge model is deduced from the TES equations. The main conceptual and practical deficiencies of this model are discussed. Then, a TES-consistent lattice model in which the cluster-lattice exchange interactions are approximated by Slater $X\alpha$ formula is presented. It is shown that this scheme, named the $PX\alpha$ model, does not suffer from most limitations of the point-charge approximation and gives a coherent and reasonable description of the equilibrium geometry of the $(CrF_6)^{4-}$ unit in $KCrF_3$. Finally, the model potential (MP) lattice model is presented and discussed. In this model the lattice ions are described by accurate local model potentials without resorting to the $X\alpha$ approximation. The MP scheme gives satisfactory equilibrium geometries and relative stabilization energies for V, Cr, and Mn impurities in $KMgF_3$.

I. INTRODUCTION

The electronic structure of transition-metal (TM) ions in ionic crystals has been analyzed in terms of cluster models for more than 25 years since the seminal paper by Sugano and Shulman[1] on $KNiF_3$. Many contributions following this work[2–19] have generally been successful in understanding some local properties of the TM compounds, i.e., those quantities essentially determined by the electron density within the cluster volume. More recently, cluster calculations incorporating noticeable theoretical refinements have been reported for TM-concentrated fluorides,[20] oxides,[21–23] chlorides and bromides,[24] as well as for TM-diluted systems.[25–29]

Although a rigorous calculation of the isolated cluster can give reasonable results for highly localized properties of these systems, the appropriate treatment of the cluster-lattice interaction becomes an essential component of the cluster model. In fact, the cluster-*in vacuo* approximation is completely improper for the analysis of questions like (a) the relative stability of different ionization states of the TM ions since different lattice effects will appear for ions of different charge; (b) electronic transitions involving delocalized states with electronic densitities spreading outside the cluster. This may be the case for many *d-s*, *d-p*, and ligand-to-metal charge-transfer transitions; (c) effects of external perturbations such as temperature jumps or external pressure since these agents modify the whole crystal; (d) the shape of potential energy surfaces since the cluster-*in vacuo* images dissociate in a way that is irrelevant in the solid. Due to the action of the crystal structure, the cluster-in-the-lattice nuclear potentials of bound electronic states should be more symmetric around their minima than their cluster-*in vacuo* counterparts. Also, the nuclear potentials of highly charged clusters like $(CuCl_6)^{5-}$ are repulsive at the cluster-*in vacuo* stage.[28]

These few examples reveal the need for a detailed analysis of the cluster-lattice interaction within the cluster model. It appears that most treatments of this interaction follow intuitive developments directed to a better description of the experiments. From this viewpoint one can claim with Brener and Callaway[21] that a rigorous basis for the cluster model in many-body theory does not yet exist, although several important notions have been advanced in this direction.[25–32] The problem of the cluster-lattice interaction is in essence a requirement for mathematical and physical consistency[30] between the structure of the cluster and that of the rest of the lattice, being then intimately related to the theoretical basis of the cluster model.

In this work we study the cluster-lattice consistency by

means of an approach that more than intuition follows basic quantum-mechanical ideas. Our purpose is to present, discuss, and apply a rigorous formulation of the cluster model derived from a first-principles description of the entire crystal and consistent with the theory of electronic separability (TES). Following the work by Parr *et al.*,[33,34] Phillips and Kleinman,[35] Szász,[36,37] Weeks and Rice,[38,39] McWeeney,[40,41] Huzinaga and his group,[42,43] and Barandiarán and Seijo,[28] we consider, in Sec. II, a cluster Hamiltonian which contains the orthogonality constraints required by the conditions of cluster-lattice separability. Using a restricted variational procedure, we discuss obtaining the Hartree-Fock (HF) cluster wave functions consistent with a given electronic structure of the lattice. We also show how to recover electronic properties of the whole crystal from the local description of its different parts.

The relevant contribution of the TES to this approach appears in the treatment of the cluster-lattice interaction. The TES gives us general rules for dealing with it while maintaining the required cluster-lattice orthogonality. Specifically, the TES shows that the cluster Hamiltonian should contain (a) an effective potential representing the quantum-mechanical nature of the lattice ions, and (b) appropriate lattice-projection operators to secure the orthogonality constraints.

These general rules leave us with two further, very important decisions to make, namely, the definition of the lattice effective potential and the choice of wave functions for the lattice ions. The first question leads to a hierarchy of approximate lattice models. The second suggests the idea of ion-lattice consistency, a goal that can be reached by following a TES-consistent, ion-in-the-lattice approach.[44]

In Sec. III we study different stages of this hierarchy of lattice models. First, there is the limit of a totally neglected cluster-lattice interaction, i.e., the cluster-*in vacuo* level, studied here with a Hartree-Fock-Roothaan (HFR) approach.[11,45] Next, we deduce from the TES equations the point-charge lattice model. We discuss how this often used but conceptually unsatisfactory approach may lead to qualitatively erroneous results, mainly because its lack of short-range or overlap interactions.

The more elaborate lattice models introduced and discussed in this hierarchy are quantum-mechanical images of the crystal lattice containing long-range Coulomb and exchange lattice interactions as well as lattice projection operators. In this way, the necessary short-range cluster-lattice interactions emerge from a rigorous formulation of the cluster-lattice separability through the orthogonality requirements.

First, we introduce a model that makes use of Slater $X\alpha$ formula to describe the cluster-lattice exchange interactions. Its application to the $(CrF_6)^{4-}$ unit in $KCrF_3$ removes the more important deficiencies of the point-charge model. Then, we discuss the model potential (MP) lattice model in which the lattice ions are represented by accurate local model potentials. We apply the MP model with very satisfactory results to the determination of the equilibrium geometry and the relative stability of several chromium, vanadium, and manganese impurities in $KMgF_3$.

Although, following Huzinaga's viewpoint,[42] our aim has been to simplify a complex solid-state problem more than to develop a sophisticated many-electron theory, we hope that the present work might contribute to show that (a) the TES can be an adequate formalism to make progress in the theoretical foundation of the cluster model, (b) the quantum effects are essential components of the cluster-lattice interaction, and (c) the TES can also be a useful guide for developing rigorous and practical treatments of the this interaction.

II. THEORY OF ELECTRONIC SEPARABILITY IN IONIC SOLIDS

A. Group wave functions and restricted variational principle

In the study of an ionic solid with an arbitrary number of electrons N, we assume the Born-Oppenheimer separation and look for the best approximate multielectron wave function $\Phi(1,N)$. Our second assumption will be that the crystal can be divided into a number of weakly interacting electronic groups $(A,B,\ldots,R,\ldots)$ with $N_A,N_B,\ldots N_R,\ldots,$ electrons, respectively. The R group contains ν_R nuclei ($\nu_R \geq 0$) and will be represented by the group electronic wave function $\Phi_R(1,N_R)$. The assumed weak interaction between any two groups does not imply that the interaction energy is small. It rather means that the electronic structure of a given group is mainly determined by the intragroup interactions.

We will write now the crystal electronic wave function in the form[41]

$$\Phi(1,N)=MA_p\{\Phi_A(1,N_A)\Phi_B(N_A+1,N_A+N_B)\cdots\}\ , \tag{1}$$

where M is a normalization constant and A_p the antisymmetrizer.

Furthermore, the group wave functions have to satisfy the strong-orthogonality restrictions[33,34]

$$\int \Phi_R^*(\mathbf{x}_1,\mathbf{x}_i,\ldots,\mathbf{x}_j,\ldots)\Phi_S(\mathbf{x}_1,\mathbf{x}_i,\ldots,\mathbf{x}_j,\ldots)d\mathbf{x}_1=\delta_{RS} \tag{2}$$

where $\mathbf{x}_i$ are the space and spin electronic coordinates and δ_{RS} the Kronecker symbol.

Under these restrictions, the total electronic energy of the crystal may be written in the form[40]

$$E=\sum_R E^R+\sum_{R>S} E^{RS}\ , \tag{3}$$

where E^R is the net energy of the R group and E^{RS} the interaction energy between groups R and S. Appropriate expressions for these energies in a Born-Oppenheimer configuration are, in hartrees,

$$E^R = T[e(R)] + V[n(R),e(R)] + V[e(R),e(R)] + V[n(R),n(R)]$$
$$= \left\langle \Phi_R \left| \sum_{i=1}^{N_R} T_i - \sum_{i=1}^{N_R} \sum_{\alpha=1}^{\nu_R} Z_\alpha r_{i\alpha}^{-1} + \sum_{i>j}^{N_R} r_{ij}^{-1} \right| \Phi_R \right\rangle + \sum_{\alpha>\beta}^{\nu_R} Z_\alpha Z_\beta R_{\alpha\beta}^{-1} , \quad (4)$$

$$E^{RS} = V[e(R),n(S)] + V[e(R),e(S)] + V[n(R),n(S)] + V[n(R),e(S)]$$
$$= \left\langle \Phi_R \left| - \sum_{i=1}^{N_R} \sum_{\beta=1}^{\nu_S} Z_\beta r_{i\beta}^{-1} \right| \Phi_R \right\rangle + \left\langle \Phi_R \left| \sum_{i=1}^{N_R} [V_C^S(i) + V_X^S(i)] \right| \Phi_R \right\rangle + \sum_{\alpha=1}^{\nu_R} \sum_{\beta=1}^{\nu_S} Z_\alpha Z_\beta R_{\alpha\beta}^{-1}$$
$$+ \left\langle \Phi_S \left| - \sum_{j=1}^{N_S} \sum_{\alpha=1}^{V_R} Z_\alpha r_{j\alpha}^{-1} \right| \Phi_S \right\rangle , \quad (5)$$

where we have used e for electronic and n for nuclear; T and V for kinetic and potential energy, respectively; indices i,j correspond to electrons, greek indices to nuclei; V_C^S and V_X^S are, respectively, the Coulomb and exchange potentials produced by the electrons of the S group. Notice that $E^{RS} = E^{SR}$.

Now we want to know how the different group wave functions and energies can be obtained. It is clear that we are not interested in all these functions. As a matter of fact, we are generally interested in a particular subsystem in which the appropriate self-consistent-field (SCF) equations can be solved. We will call this subsystem the active group A. All other groups $S \neq A$, called frozen groups, will be kept frozen in the SCF process. The best Φ_A is obtained by means of the restricted variational principle. To see this, we simply recall that all energy terms in E depending explicitly upon Φ_A can be collected in the effective energy of the A group

$$E_{\text{eff}}^A = E^A + \sum_{R \neq A} E^{AR} . \quad (6)$$

Using Eq. (6), the total energy can be written as

$$E = E_{\text{eff}}^A + \sum_{R \neq A} E^R + \sum_{R>S} E^{RS} . \quad (7)$$

Since the second and third terms in Eq. (7) are independent of Φ_A, we could obtain the best Φ_A by minimizing the effective energy E_{eff}^A while maintaining the orthogonality restrictions with the frozen groups.[42,43] This is the restricted variational principle given the best total energy of the crystal for a chosen set of frozen-group wave functions.

B. Effective Hamiltonian and projection operators

In many instances, the frozen groups can be adequately described by single Slater determinants. This is the case for a system of closed-shell frozen groups. The restricted variational procedure is then greatly simplified since the effective energy of the active group can be derived from an effective Hamiltonian[42,43]

$$E_{\text{eff}}^A = \langle \Phi_A | H_{\text{eff}}^A | \Phi_A \rangle + \sum_{S \neq A} \{ V[n(A),n(S)] + V[n(A),e(S)] \} , \quad (8)$$

where the effective Hamiltonian is

$$H_{\text{eff}}^A = \sum_{i=1}^{N_A} h_{\text{eff}}^A(i) + \sum_{i>j}^{N_A} r_{ij}^{-1} + \sum_{\alpha>\beta}^{\nu_A} Z_\alpha Z_\beta R_{\alpha\beta}^{-1} , \quad (9)$$

$$h_{\text{eff}}^A(i) = \left[T(i) - \sum_{\alpha=1}^{\nu_A} Z_\alpha r_{i\alpha}^{-1} \right] + \sum_{S \neq A} [V_{\text{eff}}^S(i) + P^S(i)] . \quad (10)$$

In Eq. (10), $V_{\text{eff}}^S(i)$ represents the potential energy of the ith electron of the active group in the field of the frozen group S. This energy contains the nuclear attraction and the Coulomb and exchange electron interactions

$$V_{\text{eff}}^S(i) = - \sum_{\beta=1}^{\nu_S} Z_\beta r_{i\beta}^{-1} + V_C^S(i) + V_X^S(i) . \quad (11)$$

If S has a closed-shell structure these terms become

$$V_C^S(i) = \sum_{g \in S} 2J_g^S , \quad (12)$$

$$V_X^S(i) = - \sum_{g \in S} K_g^S , \quad (13)$$

where g counts occupied orbitals of S. J_g^S and K_g^S are Coulomb and exchange operators, respectively.

$P^S(i)$ is an operator that projects the occupied levels of the S frozen group out of the active-group electronic wave function to be obtained in the SCF process. Thus, it represents the orthogonality restrictions holding between the active group and the S frozen group. For a closed-shell S group $P^S(i)$ becomes

$$P^S(i) = \sum_{g \in S} |\phi_g^S\rangle (-x_g^S \varepsilon_g^S) \langle \phi_g^S| , \quad (14)$$

where g runs over the occupied orbitals of S with orbital energies ε_g^S; x_g^S are the projection factors discussed below.

In the present formalism, the orthogonality constraints of Eq. (2) have been incorporated into the effective Hamiltonian by means of the projection operators. Accordingly, the best electronic wave function for the active group can be obtained by minimizing the effective energy in Eq. (8) without further constraints. Thus, the available atomic and molecular SCF programs can be easily adapted to incorporate environment effects by means of this formalism.

Finally, the interaction between the nuclei of the active

group and the electrons and nuclei of the frozen groups in Eq. (8) can be written in the form

$$\sum_{S\neq A}\{V[n(A),n(S)]+V[n(A),e(S)]\} = \sum_{S\neq A}\sum_{\alpha=1}^{\nu_A} Z_\alpha V^S_{\rm eff}(\mathbf{R}_\alpha)\ , \quad (15)$$

where $V^S_{\rm eff}(\mathbf{R}_\alpha)$ represents the effective potential of the S frozen group at the position of the α nuclei of the active group. It may be noted that only the nuclear and Coulombic terms of the effective potential contribute to the energy in Eq. (15) since there are no exchange terms between electrons and nuclei. On the other hand, this energy is a constant if the nuclear geometries of the active and frozen groups are kept fixed, but it changes when one or more of these groups undergo vibrational motions.

C. Effective potentials, description of the frozen groups, active-group basis set, and projection factors

The equations above constitute a rigorous tool for the accurate treatment of the active group under the effects of a given environment. As noted in Sec. I, two important questions must be considered in order to make this calculation feasible: (1) an approximate and accurate representation for the effective potential of each frozen group must be selected; (2) the orbital functions and energies of the frozen groups must be specified.

The first question appears because the use of the exact forms for the Coulomb and exchange operators in the effective potential would lead to the calculation of all multicenter integrals over the active and frozen groups. Then, the calculation of the electronic structure of the active group would be as expensive as that of the whole system. This question is also the origin of the hierarchy of lattice models referred to above.

The second question would generally be answered in terms of HF theory. We may note here that, in crystal simulation, the (*in vacuo*) HF solutions are not necessarily the best description of the frozen groups. SCF wave functions and orbital energies containing the effects of the crystal environment will certainly be a better choice.[44]

Selection of the projection factors x_g^S in Eq. (14) is related to the quality of the active-group basis set. Were this basis complete, the active-group function Φ_A could be orthogonal to the frozen-group functions. In this case, the expectation value of the projection operators

$$E^A(\text{proj},S)=\left\langle \Phi_A \left| \sum_{i=1}^{N_A} P^S(i) \right| \Phi_A \right\rangle \quad (16)$$

would vanish.

Höjer and Chung[46] have compared the active-group Fock equations derived from the effective Hamiltonian with the Fock equations for the whole system and have concluded the following for complete basis sets: (a) the orbital functions and energies obtained for a closed-shell active group coincide with the solutions of the complete Hamiltonian; (b) for open-shall active groups the coincidence is nearly complete; (c) the projection factors are $x_g^S=2$.

In crystal simulation, however, one has to use reduced basis sets. If the active-group basis does not have functions in regions where the frozen-group orbitals have appreciable amplitude, the required orthogonality will be incomplete. Then, the projection energy [Eq. (16)] no longer vanishes and becomes an approximate nonorthogonality correction to the effective energy.[47] Under such circumstances, some reduction of the x_g^S's may be considered.[47] Such reduction may give results resembling those obtained when the exchange interactions between active and frozen groups are neglected.[48] A judicious selection of the active-group basis set would take into consideration the orthogonality requirements with the chosen frozen-group functions.

D. Global properties and cluster models

From the above discussion we see that the cluster model can be readily formulated in the context of the TES. We identify the active group with the cluster and the remaining lattice ions with the frozen groups. Once the wave function Φ_A and the effective energy $E^A_{\rm eff}$ are obtained through a cluster calculation, the local properties of the crystal can be computed. It is interesting to recall that global properties of the system can also be computed once the electronic structure (Φ_A and $E^A_{\rm eff}$) of each group has been determined. To see this, it is helpful to introduce the *additive energy* of a group A,

$$E^A_{\rm add}=E^A+\tfrac{1}{2}\sum_{S\neq A}E^{AS}\ , \quad (17)$$

which is immediately obtained as a by-product in the calculation of $E^A_{\rm eff}$ and Φ_A. We can see that for an AB crystal the total energy becomes

$$E=E^A_{\rm add}+E^B_{\rm add}\ . \quad (18)$$

This equation has been written in a graphical fashion in Fig. 1. In general, for the $A_aB_bC_c\ldots$ crystal we have

$$E=aE^A_{\rm add}+bE^B_{\rm add}+cE^C_{\rm add}+\cdots\ . \quad (19)$$

Notice that Eqs. (18) and (19) hold for molecular systems and infinite crystals as well. The total energy obtained through these equations can then be used to com-

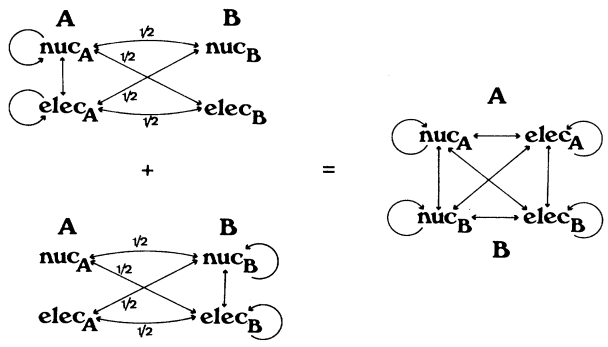

FIG. 1. Graphical representation of the relationship between the additive energies $E^A_{\rm add}$, $E^B_{\rm add}$ and the total energy of the AB system [Eq. (18)].

pute the cohesive energy and elastic constants of the crystal. On the other hand, since the global wave function is given by Eq. (1), the orthogonality conditions in Eq. (2) lead to a first-order density function

$$\rho(\mathbf{r})=\sum_S \rho^S(\mathbf{r}) , \tag{20}$$

where $\rho^S(\mathbf{r})$ is the first-order density for the S group

$$\rho^S(\mathbf{r})=N_S \int \Phi_S^*(1,N_S)\Phi_S(1,N_S)ds_1 d\mathbf{x}_2 \cdots d\mathbf{x}_{N_S} . \tag{21}$$

In this way, we can obtain the second-order density and the transition densities for the whole system and, from them, the one- and two-particle properties. In summary, once we have chosen a given partition for the system we compute the group wave functions and energies through the restricted variational principle; from this information we can recover the global properties of the system and make an appraisal of the selected partition.

To end this section, we will make a final remark on the equilibrium geometry of the TM cluster in a crystal, although the argument is general enough to be useful for other crystalline systems as well. The equilibrium geometry may be considered either as a local or a global property. The present formalism gives the appropriate equations. To see this, let us assume, for simplicity, that the geometry of a crystal is given by the **a** vector and that of the active group in this crystal by the **R** vector. Equation (7) can now be written in the form

$$E(\mathbf{R},\mathbf{a})=E^A_{\text{eff}}(\mathbf{R},\mathbf{a})+E^A_{\text{rest}}(\mathbf{a}) , \tag{7'}$$

where E^A_{rest} does not contain any contribution from the active group and is then independent of **R**. If we fix the geometry of the crystal at a given value of **a**, we could obtain the equilibrium geometry of this group by minimizing its effective energy with respect to **R**. This procedure corresponds to the treatment of the equilibrium geometry as a local property and gives a different value of **R** for each **a**. On the other hand, if the geometry is considered as a global property, we have to find the optimum values for **R** and **a**. Then, the quantity to be minimized is no longer the effective energy but the total energy of the crystal.

III. $(MF_6)^{n-}$ CLUSTERS IN CUBIC FLUOROPEROVSKITES

Many transition-metal compounds with the AMF_3 cubic-fluoroperovskite structure are known. In TM-concentrated crystals with this formula, M^{2+} is the transition-metal ion and A^+ is most often an alkali cation. The M^{2+} cation is surrounded by an octahedral coordination of F^- ions (see Fig. 2). In TM-doped perovskites, the M^{2+} site is occupied by a M^{z+} TM ion. Thus, in this section we deal with $(MF_6)^{n-}$ TM units ($n=6-z$) embedded in the perovskite lattice.

A. Hartree-Fock-Roothaan calculation of the $(MF_6)^{n-}$ cluster *in vacuo*

The electronic structure of the $(MF_6)^{n-}$ units *in vacuo* has been computed here with the cluster methodology

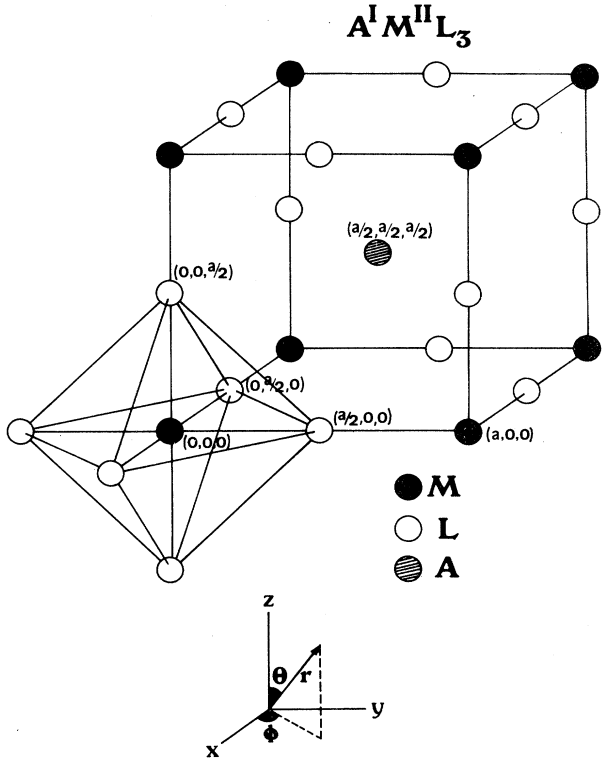

FIG. 2. Crystal structure of the cubic fluoroperovskite showing the octahedral coordination of the M^{2+} ion.

developed by Richardson *et al.*[11] which is an application of the open-shell HFR formalism[49] to the problem of a TM ion in a crystal lattice. For the sake of computational economy, the frozen-core approximation is adopted.[11] Core-valence orthogonalities are fulfilled by using adequate core-projection operators in the Fock Hamiltonian, as suggested by the TES.[45,50] Ligand-ligand interactions are accurately computed by means of the renormalization correction described by Kalman and Richardson[51] and adapted by Francisco to the last version of this methodology.[52] As in an earlier work, we used the reduced Slater-type orbital (STO) basis set of Richardson *et al.*[53,54] for the metallic cations. The fluoride basis is that of Ref. 14. In all calculations reported here the valence space is made of the 3*s*, 3*p*, 3*d*, 3*d'*, 4*s*, and 4*p* atomic orbitals (AO's) of the metal ion, and the 2*s* and 2*p* AO's of the six fluoride ions. 3*d'* is the inner STO of the regular 2ζ AO of Ref. 53.

From our experience on these systems, we know that cluster-*in vacuo* calculations of these computational characteristics give (a) equilibrium *M-L* distances within the experimental range determined in families of compounds;[55] (b) accurate *d-d* electronic spectra and reasonable *M-L* dependence of the optical parameters;[56,57] (c) a consistent picture of the metal-ligand covalency and its variation with the *M-L* separation;[58] (d) 3*d*-4*s* transitions in reasonable agreement with observed data;[59] (e) first-order density matrices and deformation electron densities in qualitative agreement with well-known bonding mechanisms, such as the 3*d* orbital symmetrization and radial

deformation, *M-L* covalency, ligand hybridization, etc.[60]

It then appears that these cluster-*in vacuo* calculations are a reasonable starting point for the analysis of lattice effects on the electronic structure of TM clusters.

B. Point-charge lattice model

Simulation of the lattice ions surrounding the cluster by motionless point charges obeying Coulomb's Law has been a common practice in cluster-type calculations on transition-metal systems. References 20, 23, 26, and 61 are recent examples. Here we will discuss the relationship between this approximation and the rigorous equations of the TES presented above. Furthermore, we will give some numerical examples that show some of the more important conceptual and practical limitations of the point-charges model.

In the present formulation, the interaction between a cluster electron and a lattice ion has four terms [Eqs. (10) and (11)]: nuclear attraction, Coulomb repulsion, exchange interaction, and lattice-ion projection. If the electrons of the lattice ion collapse into their nucleus, the nuclear-attraction and Coulomb terms would merge into a single nuclear-attraction term corresponding to the point-charge ion resulting from the electronic collapse. Also, we could expect that the remaining exchange and projection terms disappear in the collapsing process, given their intrinsic electronic nature.

It may be interesting to model the point-charge approximation by means of some functional representation of the lattice ions. This modeling could be worked out in a number of ways. Here we represent the electronic collapse by describing the lattice-ion orbitals with Dirac-δ functions

$$\phi_g^S(\mathbf{r})=\delta(|\mathbf{r}-\mathbf{R}_S|)\ , \tag{22}$$

where $\mathbf{R}_S$ is the position vector of the S lattice ion. Using Eq. (22), the Coulomb lattice potential becomes

$$\begin{aligned} V_C^S(\mathbf{r}) &= \sum_{g\in S} N_g^S \int \phi_g^S(\mathbf{r}_2)^* |\mathbf{r}-\mathbf{r}_2|^{-1} \phi_g^S(\mathbf{r}_2) d\mathbf{r}_2 \\ &= \sum_{g\in S} N_g^S \int \delta^*(|\mathbf{r}_2-\mathbf{R}_S|)|\mathbf{r}-\mathbf{r}_2|^{-1}\delta(|\mathbf{r}_2-\mathbf{R}_S|)d\mathbf{r}_2 \\ &= \sum_{g\in S} N_g^S |\mathbf{r}-\mathbf{R}_S|^{-1} = N_S|\mathbf{r}-\mathbf{R}_S|^{-1}\ , \end{aligned} \tag{23}$$

where N_g^S is the electron population of ϕ_g^S. Equation (23) and the nuclear potential of the lattice ion form the pointlike nuclear attraction

$$V_{\text{eff}}^S(\mathbf{r})=-(Z^S-N_S)|\mathbf{r}-\mathbf{R}_S|^{-1}\ . \tag{24}$$

The exchange interaction between lattice ions and a cluster wave function becomes

$$\begin{aligned} \langle\psi|V_X|\psi\rangle &= -\sum_{g\in S}\int \psi^*(\mathbf{r}_1)\delta(|\mathbf{r}_1-\mathbf{R}_S|)d\mathbf{r}_1 \int \delta^*(|\mathbf{r}_2-\mathbf{R}_S|)\psi(\mathbf{r}_2)|\mathbf{r}_1-\mathbf{r}_2|^{-1}d\mathbf{r}_2 \\ &= -\sum_{g\in S}\int \psi^*(\mathbf{r}_1)\delta(|\mathbf{r}_1-\mathbf{R}_S|)|\mathbf{r}_1-\mathbf{R}_S|^{-1}d\mathbf{r}_1\psi(\mathbf{R}_S) \\ &= -\sum_{g\in S}|\psi(\mathbf{R}_S)|^2|\mathbf{R}_S-\mathbf{R}_S|^{-1}\ . \end{aligned} \tag{25}$$

If the cluster-lattice orthogonality is satisfied, the $\langle\phi_g^S|\psi\rangle$ overlap integral must vanish. Using Eq. (22), this integral becomes

$$\langle\phi_g^S|\psi\rangle=\int\delta^*(|\mathbf{r}-\mathbf{R}_S|)\psi(\mathbf{r})d\mathbf{r}=\psi(\mathbf{R}_S)\ . \tag{26}$$

Equation (26) tells us that the exchange matrix element in Eq. (25) is a sum of 0/0 terms that will vanish if the cluster-lattice overlap goes to zero faster than the linear denominator. This matrix element will tend to $-\infty$ if the cluster-lattice orthogonality is not completely achieved, i.e., if $\psi(\mathbf{R}_S)\neq 0$. Analogous results are obtained for the off-diagonal matrix elements of the exchange interaction.

Furthermore, Eq. (26) gives the following result for the matrix elements of the lattice projection:

$$\begin{aligned} \langle\psi'|P^S|\psi\rangle &= \sum_{g\in S}\langle\psi'|\phi_g^S\rangle(-x_g^S\varepsilon_g^S)\langle\phi_g^S|\psi\rangle \\ &= \psi'(\mathbf{R}_S)^*\psi(\mathbf{R}_S)\sum_{g\in S}(-x_g^S\varepsilon_g^S)\ . \end{aligned} \tag{27}$$

The equation shows the difficulty of evaluating the orbital energy associated with a Dirac-δ orbital. Thus, Dirac-δ representation of the lattice ions drives us to important conceptual problems related to the exchange and lattice-projection terms. This fact is not astonishing, given the specific quantum origin of these terms.

In summary, the point-charge Hamiltonian is given by a simplified form of Eq. (10), namely,

$$h_{\text{eff}}(\text{cluster})=h(\text{cluster})+V_{\text{ext}}(\mathbf{r})\ , \tag{28}$$

where h(cluster) is the one-electron Hamiltonian for the cluster *in vacuo*,[11] and $V_{\text{ext}}(\mathbf{r})$ the Madelung potential of the crystal lattice at the point $\mathbf{r}$, minus the contributions from the ions forming the cluster

$$\begin{aligned} V_{\text{ext}}(\mathbf{r}) &= -\sum_{S\notin\text{cluster}}(Z^S-N_S)|\mathbf{r}-\mathbf{R}_S|^{-1} \\ &= -\sum_{S\notin\text{cluster}} z^S|\mathbf{r}-\mathbf{R}_S|^{-1}\ . \end{aligned} \tag{29}$$

In Eq. (29), $z^S=Z^S-N_S$ is the point charge of the S ion. The sum in this equation runs over all ions in the lattice excluding the components of the cluster. It can be

computed adequately by means of the Ewald method.[62–65] Once we have calculated numerical values of this lattice potential throughout the cluster volume, we can use an appropriate analytical expression to represent them as accurately as desired. The form of this analytical representation should be chosen with two ideas in mind. First, it should be particularly accurate in those regions of the cluster where the electron density is high. Second, its matrix elements within the cluster basis set should be analytically calculable without difficulty. Details are given in the Appendix.

The lattice potential $V_{\text{ext}}(\mathbf{r})$ has two characteristics that deserve comment. First, it is a homogeneous function of the electron coordinates of degree -1. Thus, if $\mathbf{a}=(a,b,c)$ is a unit-cell vector, we have

$$V_{\text{ext}}(s\mathbf{r};s\mathbf{a})=s^{-1}V_{\text{ext}}(\mathbf{r},\mathbf{a}) , \tag{30}$$

where s is a scale factor.

Second, $V_{\text{ext}}(\mathbf{r})$ must transform according to the totally symmetric irreducible representation of the point group of the cluster. Otherwise, it would connect cluster wave functions belonging to different representations and would reduce the symmetry of the cluster Hamiltonian.

Let us see now results for the electronic ground state of the $(CrF_6)^{4-}$ cluster embedded in the point-charge lattice of $KCrF_3$. This crystal has a high-temperature perovskite phase with $a=4.158\pm0.004$ Å (7.857±0.008 bohr) (Ref. 66). In parts (a) and (b) of Fig. 3 we show the

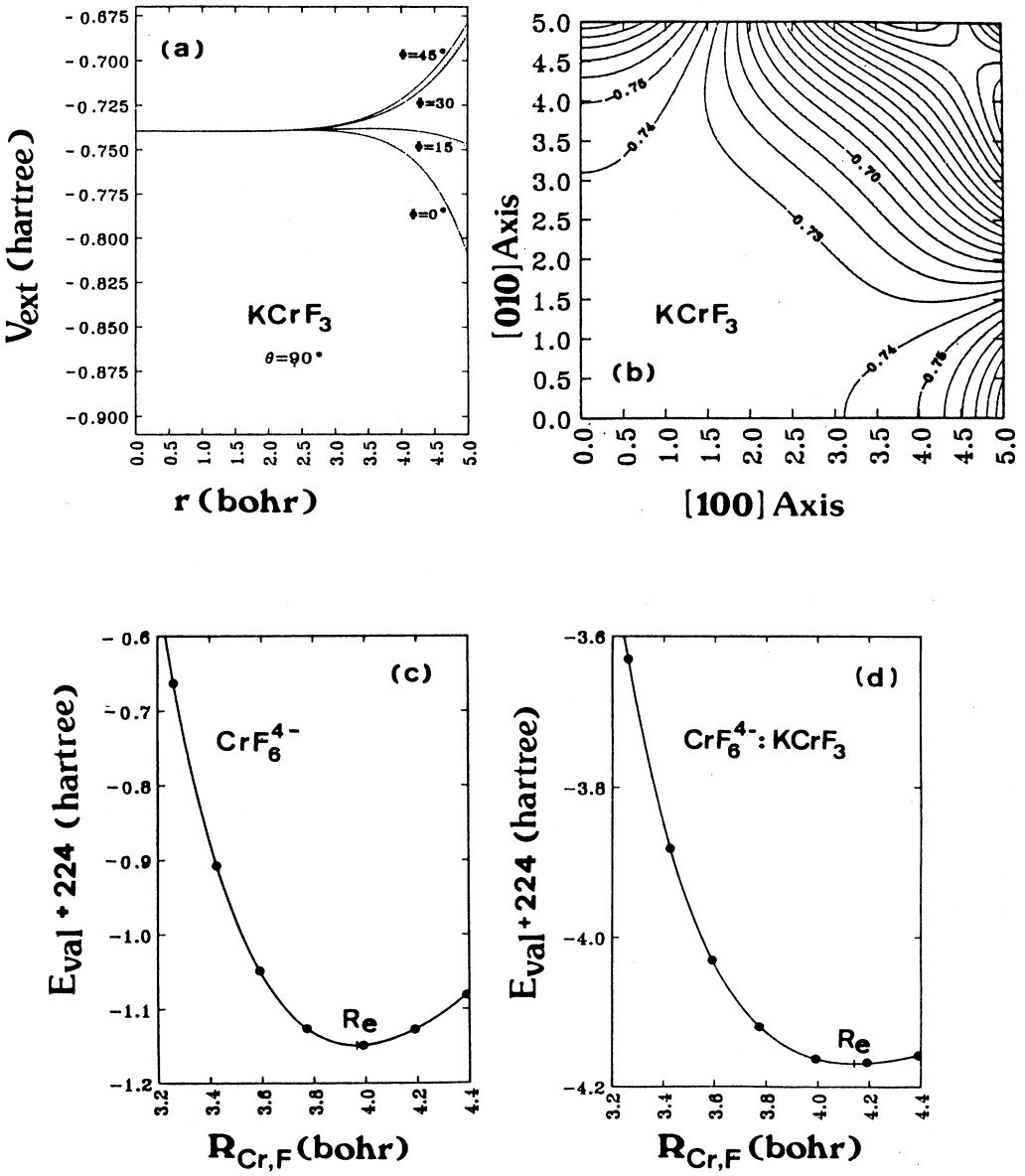

FIG. 3. (a) Point-charge lattice potential for $KCrF_3$ in selected directions, and (b) in the xy plane of the cluster. (c) Ground-state nuclear potential for the $(CrF_6)^{4-}$ unit *in vacuo*, and (d) in $KCrF_3$.

TABLE I. Cluster valence energy of the $(CrF_6)^{4-}$ unit *in vacuo* E_0 and embedded in the point-charge lattice E_{PC} for three values of the cell constant **a**. [E_{CL}(PC) is the cluster-lattice energy computed as $E_{CL}(PC)=E_{PC}-E_0$. All numbers in atomic units.]

				R(Cr-F)				
Calculation	Quantity	3.26	3.425	3.59	3.772	3.99	4.19	4.39
In vacuo	E_0+224	−0.663 89	−0.908 18	−1.049 72	−1.126 76	−1.149 17	−1.127 86	−1.081 68
$KCrF_3$	$E_{PC}+224$	−3.744 73	−3.997 79	−4.151 06	−4.245 64	−4.297 85	−4.315 62	−4.324 19
(**a**=4.010 Å)	E_{CL}(PC)	−3.080 84	−3.089 61	−3.101 34	−3.118 88	−3.148 68	−3.187 76	−3.242 51
$KCrF_3$	$E_{PC}+224$	−3.630 93	−3.881 24	−4.030 79	−4.119 75	−4.162 32	−4.167 36	−4.157 97
(**a**=4.158 Å)	E_{CL}(PC)	−2.967 04	−2.973 06	−2.981 07	−2.992 99	−3.013 15	−3.039 50	−3.076 29
$KCrF_3$	$E_{PC}+224$	−3.570 43	−3.819 60	−3.967 61	−4.054 25	−4.092 85	−4.092 65	−4.075 90
(**a**=4.242 Å)	E_{CL}(PC)	−2.906 54	−2.911 42	−2.917 89	−2.927 49	−2.943 68	−2.964 79	−2.994 22

form of $V_{ext}(\mathbf{r})$ along the *xy* plane for this phase. We can observe that this potential is practically flat in the range $0 \le r \le 2.5$ bohr around Cr^{2+} ion. Farther away from this ion, $V_{ext}(\mathbf{r})$ decreases along the 100 and nearby directions, stabilizing the negative charges more as their separation from the metal ion becomes larger. On the contrary, $V_{ext}(\mathbf{r})$ increases along the 110 and nearby directions, raising the energy of the negative charges. Since the cluster electron density concentrates along the *M-L* (100) axes, the behavior of $V_{ext}(\mathbf{r})$ along these directions will dominate the cluster-lattice energy. Moreover, the total electron-lattice energy should be larger, in absolute value, than the total nucleus-lattice energy because the total charge of the cluster is −4 a.u. All these qualitative arguments suggest that the cluster-in-$KCrF_3$ value of $R_e(Cr^{2+}\text{-}F^-)$ should be larger than the cluster-*in vacuo* value. This is indeed the result of our HFR calculations, as the ground-state energy curves depicted in Fig. 3 reveal. The cluster total energy decreases by about 3 hartree (80 eV) when this lattice potential is included in the calculation.

The effects of the lattice potential in the equilibrium properties of the cluster are the following. The *M-L* distance increases from $R_e(vacuo)=2.099$ Å to $R_e(KCrF_3)=2.191$ Å. The a_{1g} vibration frequency decreases from $\omega_e(vacuo)=488$ cm^{-1} to $\omega_e(KCrF_3)=334$ cm^{-1}. The observed value for $R_e(KCrF_3)$ is 2.079±0.002 Å.[66]

The nuclear potential obtained with this point-charge lattice [Fig. 3(d)] is noticeably asymmetric with respect to a vertical axis passing through R_e. However, a rather symmetric nuclear potential should be expected since the fluoride ions of the cluster are located in the middle of the segment connecting two Cr^{2+} ions. Thus, this feature is surely in error.

At this point, it is interesting to show a further deficiency of the point-charge lattice potential in $KCrF_3$. Let us imagine a breathing vibration of the whole crystal and let us compute the cluster nuclear potential for different values of the cell constant **a**, without making any other change in the crystal structure. Results for **a**=4.010, 4.158, and 4.242 Å can be seen in Table I and Fig. 4. According to this amazing result, the size of the cluster increases when the cell constant decreases, and *vice versa*. This unphysical response is not a curiosity but a consequence of the form of $V_{ext}(\mathbf{r})$ and its scaling property, Eq. (30). We find analogous results for $(VF_6)^{4-}$ and $(MnF_6)^{4-}$. They reveal the need for short-range contributions to $V_{ext}(\mathbf{r})$. In this numerical experiment, these contributions will be larger for the smaller lattice and would restore the expected response. As noted in Sec. I, the short-range lattice potential can be incorporated in the cluster calculation in many different ways. In the rest of the paper we will analyze the effects of the particular choice suggested by the TES.

C. *PXα* lattice model

This TES-consistent lattice model is a quantum-mechanical representation of the crystal lattice defined as

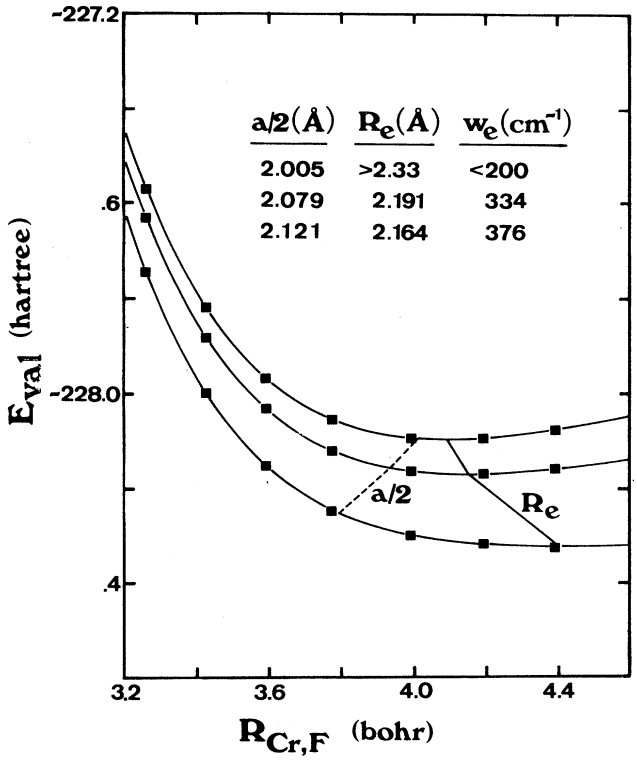

FIG. 4. Ground-state nuclear potential for the $(CrF_6)^{4-}$ unit in the point-charge lattice of $KCrF_3$ computed for three different values of the cell constant **a** [**a**/2=2.005 (lower curve), 2.079 (middle curve), and 2.121 Å (upper curve)].

follows:

(a) Each lattice ion is described by its ground-state HF orbital wave functions and energies.

(b) The Coulomb potential produced by the S lattice ion is given by

$$V_C^S(r_1)=\int \rho^S(r_2)r_{12}^{-1}d\tau_2 , \tag{31}$$

where

$$\rho^S(r)=(1/4\pi)\sum_{j,l\in S} N_{jl}^S[R_{jl}^S(r)]^2 \tag{32}$$

is the radial density of the S ion. The sum in Eq. (32) runs over the orbitals of the S ion, with radial functions $R_{jl}^S(r)$ and electron occupation N_{jl}^S.

(c) The exchange potential from the S lattice ion is given by the Slater local $X\alpha$ approximation[67]

$$V_X^S=V_{X\alpha}^S=-3\alpha[3\rho^S(r)/8\pi]^{1/3} . \tag{33}$$

(d) The lattice-projection operators, Eq. (14), are defined in terms of the HF solutions referred to in (a).

A very similar approach has been followed by Katsuki and Inokuchi[68] in their work on core model potentials for atomic and molecular $X\alpha$ calculations.

Equations (31) and (32) are exact for a closed-shell ion. For open-shell ions, Eq. (32) gives the electronic density averaged over the m_l components of the open shell. Equations (31)–(33) are then applicable to closed- and open-shell ions. As it is the case for the point-charge approximation, the $PX\alpha$ model is applicable to crystals formed of open-shell ions for which the TES equations are not proved to be rigorous.

According to the definition, the $PX\alpha$ effective potential is spherically symmetric. To examine its asymptotic behavior we consider its associated effective charge $Z_{\mathrm{eff}X\alpha}^S(r)=-rV_{\mathrm{eff}X\alpha}^S(r)$, which has the following limits:

$$\lim_{r\to 0} Z_{\mathrm{eff}X\alpha}^S(r)=Z^S , \tag{34}$$

$$\lim_{r\to\infty} Z_{\mathrm{eff}X\alpha}^S(r)=Z^S-N_S=z^S . \tag{35}$$

This means that at very short distances of the S nucleus the electronic screening vanishes. At very large distances the screening is complete, i.e., the S ion becomes a point charge whose magnitude is given by its atomic number minus its electron number.

The spherical symmetry permits an accurate approximation of $V_{\mathrm{eff}X\alpha}^S(r)$ by means of a model potential. We have used the form proposed by Bonifacic and Huzinaga[69]

$$V_{\mathrm{mod}}^S(r_S)=-(Z^S-N_S)r_S^{-1}\left[1+\sum_{k=1}^{M} A(k,S)r_S^{n(k,S)}\exp[-\alpha(k,S)r_S]\right] , \tag{36}$$

where $r_S=|\mathbf{r}-\mathbf{R}_S|$ and $A(k,S)$, $n(k,S)$, and $\alpha(k,S)$ fitting parameters for a chosen value of M. Once we have determined the effective potentials for all different lattice ions, the lattice effective potential at the point $\mathbf{r}$ of the cluster region is given by

$$V_{\mathrm{ext}}(r)=\sum_{S\notin\text{cluster}} V_{\mathrm{eff}X\alpha}^S(r_S)=\sum_{S\notin\text{cluster}} V_{\mathrm{mod}}^S(r_S) \tag{37}$$

and it can be represented by an accurate analytical expression, as detailed in the Appendix.

Let see now the results of our calculations with the $PX\alpha$ model for $(CrF_6)^{4-}$ in $KCrF_3$. The K^+ ions have been represented by the HF solutions of Clementi and Roetti[70] but, for consistency, the Cr^{2+} and F^- lattice ions have been described with the cluster-*in vacuo* basis. A value of $\alpha=\frac{2}{3}$ has been taken for the exchange potential.

In Fig. 5 we plot the effective charges for these three ions, as well as the Coulomb contribution $Z_C^S=-rV_C^S$, and the exchange charge $Z_{X\alpha}^S=-rV_{X\alpha}^S$. From these plots we observe that the Coulomb charges reach the asymptotic value $-N_S$ for $r\cong 2$ bohr. The exchange contributions are smaller and considerably more long ranged. In consequence, the effective charge is mainly determined by the exchange charge for $2\le r\le 7$ bohr. At distances larger than about 6–7 bohr these effective charges merge with their pointlike asymptotic value.

The lattice-projection operators have been computed with projection factors $x_g^S=1$. As remarked at the end of Sec. II C, using this instead of the $x_g^S=2$ choice may be adequate when a reduced basis set is adopted. Whereas

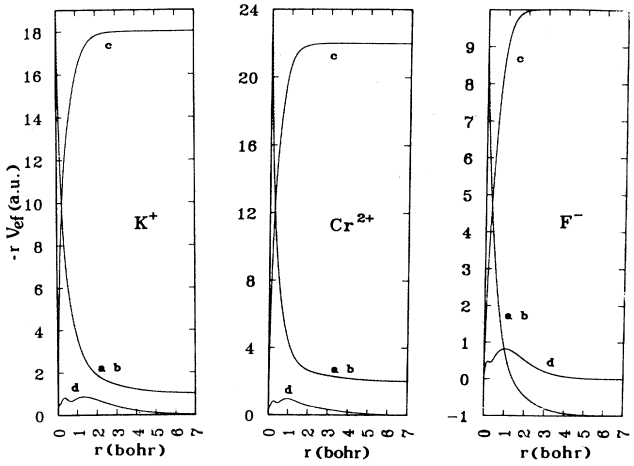

FIG. 5. (a) Effective charge $Z_{\mathrm{eff}X\alpha}=-rV_{\mathrm{eff}X\alpha}$, (b) model-potential charge $Z_{\mathrm{mod}}=-rV_{\mathrm{mod}}$, (c) Coulomb charge $Z_C=-rV_C$, and (d) exchange charge $Z_{X\alpha}=-rV_{X\alpha}$ for the K^+, Cr^{2+}, and F^- ions.

the analysis by Höjer and Chung[46] suggests the adoption of the second choice, some advantages[45] may be obtained by following the first one. Using the soft projection ($x_g^S=1$) in calculations of this type may be viewed as a partial remedy to the incomplete basis set of the cluster and to the approximate treatment of the cluster-lattice exchange. As we discuss in detail elsewhere,[71] the soft projection may give rise to values of R_e a few hundredths of an angstrom larger than those obtained with $x_g^S=2$, since the lattice projection acts as a repulsive potential on the part of the crystal lattice.

The matrix elements of the lattice projector contain the product of two cluster-lattice overlap integrals. These terms decrease exponentially with the separation of the lattice ion from the cluster. This means that only the closer ionic shells do contribute to the expectation values of the lattice projectors. With the basis set used in the present calculation we find that the 8 K^+ ions at the $(\pm a/2,\pm a/2,\pm a/2)$ positions and the 6 Cr^{2+} ions at $(\pm a,0,0)$ form the dominant contributions to the lattice projection. The 24 F^- ions at $(\pm a,\pm a/2,0)$ are also important. The contributions from the remaining lattice ions are smaller than 10^{-5} hartree and have been neglected.

We collect in Table II ground-state total energies, lattice-projector expectation values, and effective potential energies for $(CrF_6)^{4-}$ in $KCrF_3$ at three different values of the cell constant. We observe that the lattice projection represents a small but relevant contribution to the nuclear potential, given its fast variation with the *M-L* coordinate R and the cell constant **a**. As noted above, it acts as a repulsive interaction that tends to reduce the cluster-*in vacuo* value of R_e.

The effective potential makes the cluster total energy some 4–5 hartree more negative. Its expectation value increases, in absolute value, with the cluster size and turns out to be 1–2 hartree more negative than that corresponding to the point-charge scheme. Since the molecular orbitals (MO's) obtained in the point-charge and $PX\alpha$ calculations are very similar, this enhancement may be attributed to more intense Coulomb interactions in the latter description, as well as to the action of the exchange

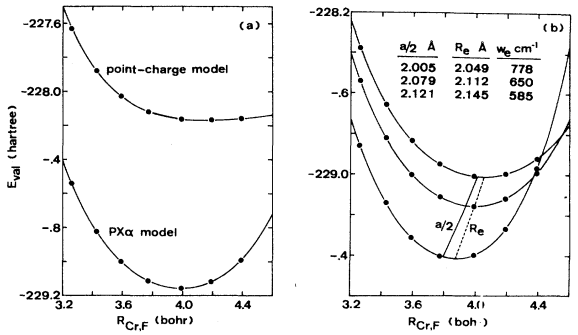

FIG. 6. Ground-state nuclear potential for the $(CrF_6)^{4-}$ unit in $KCrF_3$. (a) Results for point-charge and $PX\alpha$ lattice models. (b) $PX\alpha$, model results for three values of the lattice cell constant **a**.

potential. The effective lattice potential acts as an attractive interaction on the part of the crystal lattice that tends to increase the cluster-*in vacuo* value of R_e.

The more significant differences between the point-charge and $PX\alpha$ lattice models in the determination of the cluster nuclear potential can be seen in Fig. 6(a). The $R_e(KCrF_3)$ obtained with the latter is 2.112 Å, in good agreement with the observed 2.079±0.002 Å.[66] The reduction in $R_e(KCrF_3)$ with respect to the point-charge value (2.191 Å) is clearly due to the action of the lattice projection. Furthermore, the $PX\alpha$ nuclear potential is much more symmetric than that obtained with the point-charge model, in agreement with the expectations commented above. Compared with the in cluster-*in vacuo* stage, the $PX\alpha$ lattice model produces a slight increase in the value of R_e (0.013 Å) and a noticeable increment in the vibration frequency (162 cm^{-1}).

Using the $PX\alpha$ lattice model, we have repeated the numerical experiment of lattice vibration discussed above. Results can be seen in Fig. 6(b). It is satisfactory to see that these nuclear potentials are highly symmetric around the equilibrium position and that the predicted values for R_e follow correctly the variation of the cell

TABLE II. Valence energy of the $(CrF_6)^{4-}$ unit in the $PX\alpha$ lattice $E_{PX\alpha}$ for three values of the cell constant **a**. [$E_{CL}(PX\alpha)$ is the cluster-lattice energy computed as $E_{PX\alpha}-E_0$. $\langle P\rangle$ is the expectation value of the lattice-projection operator. All numbers in atomic units; **a**/2 in Å.]

		R(Cr-F)						
a/2 (Å)	Quantity	3.26	3.425	3.59	3.772	3.99	4.19	4.39
	$E_{PX\alpha}+224$	−4.861 02	−5.141 93	−5.312 31	−5.403 85	−5.397 87	−5.267 68	−4.966 22
2.005	$\langle P\rangle$	0.163 23	0.221 21	0.301 62	0.429 69	0.669 36	1.023 93	1.590 56
	$E_{CL}(PX\alpha)$	−4.360 36	−4.454 96	−4.564 21	−4.706 78	−4.918 06	−5.163 75	−5.475 10
	$E_{PX\alpha}+224$	−4.540 39	−4.823 40	−5.001 36	−5.112 20	−5.156 37	−5.119 08	−4.990 70
2.079	$\langle P\rangle$	0.088 78	0.120 30	0.163 64	0.232 13	0.359 09	0.545 05	0.839 91
	$E_{CL}(PX\alpha)$	−3.975 28	−4.035 52	−4.115 28	−4.217 57	−4.366 29	−4.536 27	−4.748 93
	$E_{PX\alpha}+224$	−4.375 47	−4.657 38	−4.835 87	−4.950 59	−5.007 67	−4.996 66	−4.919 77
2.121	$\langle P\rangle$	0.062 60	0.084 85	0.115 33	0.163 37	0.252 12	0.381 55	0.585 72
	$E_{CL}(PX\alpha)$	−3.774 18	−3.834 05	−3.901 48	−3.987 20	−4.110 62	−4.250 35	−4.423 81

constant. Moreover, the difference between R_e and $\mathbf{a}/2$ in this imaginary crystal is always smaller than 0.05 Å, indicating a good agreement between model and experiment. We also notice that the effective energy of the cluster decreases, and the vibration frequency increases, for smaller values of the cell constant. As commented in Sec. II, the optimum value of the cell constant **a** cannot be obtained from the effective energy of the cluster: We would need the total "molecular" energy of the crystal. In view of all these results, we can conclude that the $PX\alpha$ lattice model gives a qualitatively correct and quantitatively reasonable description of the equilibrium geometry of this chromium cluster in $KCrF_3$.

We will finally refer to some spectral properties of this cluster whose sensitivity to the modeling of the external lattice may be smaller than that found for the ground-state nuclear potential.

First, in Fig. 7 we depict the orbital energies of the cluster valence shell at several states of our calculation. All entries correspond to $R(Cr^{2+}\text{-}F^-)=3.99$ bohr. In this figure we observe (stage *B*) that the valence levels of the free Cr^{2+} ion increase their energy by about 40 eV, and those of the F^- ion by some 10 eV, as a consequence of the pure electrostatic interactions with the rest of the cluster ions. Stage *B* gives a reasonable estimation of the cluster-*in vacuo* description (stage *C*), although the splitting of the levels is missing. The lattice interactions decrease the energy of all these valence levels by some 20 eV. Differences between the point-charge (stage *D*) and $PX\alpha$ (stage *E*) lattices are very small, although in some cases they can be of 2 eV. Although the relative separation of these levels changes very slightly in passing from *vacuo* to the lattice, the position of the 3*d* levels with respect to the 2*p* fluoride band may be modified. For instance, the mainly 3*d*, half-filled $2t_{2g}$ level is located 0.12 (stage *C*) and 0.03 eV (stage *D*) below the fully occupied $6t_{1u}$ ($2p\pi_L$) level, respectively. This slight departure from the *aufbau* principle is neither unusual nor inconsistent with the description of the optical spectrum in terms of multielectron wave functions and energies. In any case, in the $PX\alpha$ calculation (stage *E*) this ordering is reversed and the 3*d* level appears 1.04 eV above the top of the filled band.

Second, we present in Fig. 8 the dependence of the $t_{2g}(3)e_g(1)\text{-}{}^5E_g \rightarrow t_{2g}(2)e_g(2)\text{-}{}^5T_{2g}$ electronic transition of this cluster with the metal-ligand distance R. This transition, called Δ or $10Dq$, varies with R in a way that can be accurately described by the inverse-power law $\Delta/\Delta_0=(R_0/R)^n$. The three lines in Fig. 8 correspond to (a) cluster-*in vacuo* calculations, (b) point-charge lattice model, and (c) $PX\alpha$ lattice model. The small ordinate at the origin is a measure of the accuracy of the inverse-power equation. This equation is followed slightly better when the lattice effects are included, particularly for the $PX\alpha$ model. According to this calculation, the best values of n are 5.28 (*vacuo*), 5.45 (point charges), and 5.63

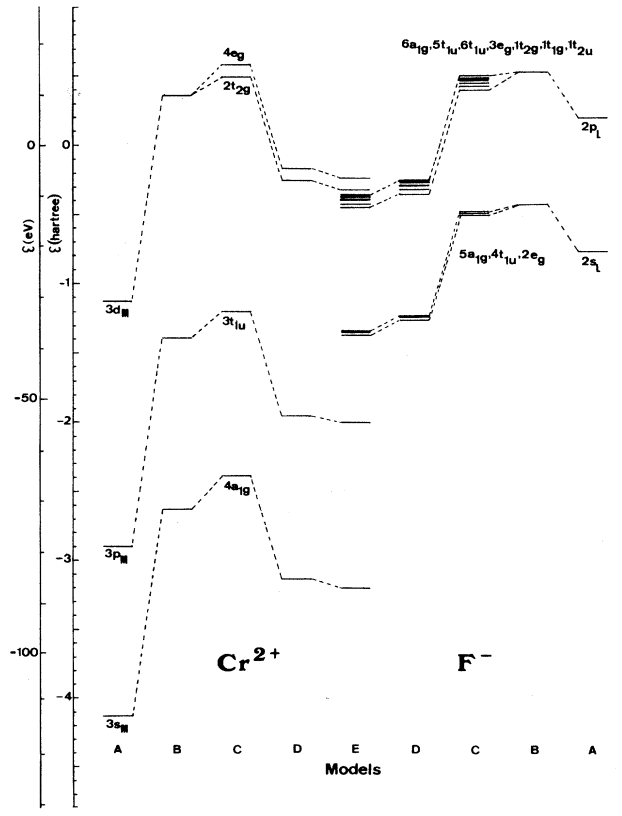

FIG. 7. Orbital energies of the cluster valence shell at several stages of the calculation ($R=3.99$ bohr). *A*: free ion. *B*: *A* plus the effect of a point-charge cluster. *C*: $(CrF_6)^{4-}$ *in vacuo*. *D*: $(CrF_6)^{4-}$:$KCrF_3$, point-charge lattice. *E*: $(CrF_6)^{4-}$:$KCrF_3$, $PX\alpha$ lattice.

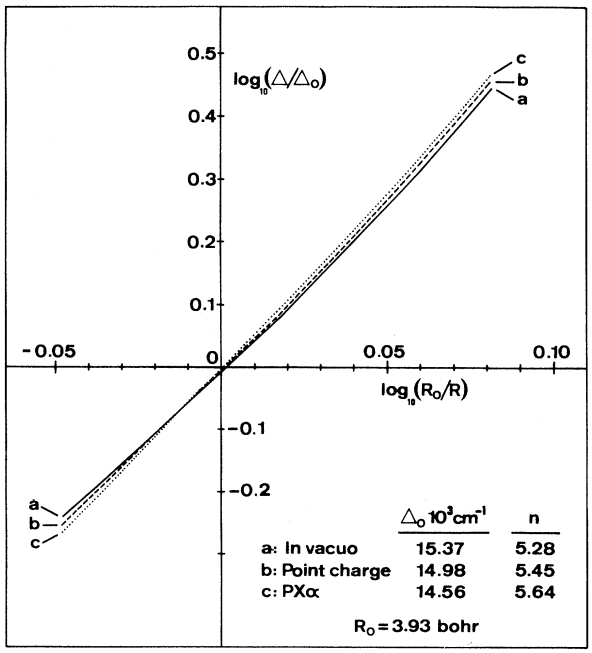

FIG. 8. Variation of the transition energy $\Delta=10Dq=E({}^5T_{2g})-E({}^5E_g)$ with the metal-ligand distance R according to several calculations on the $(CrF_6)^{4-}$ unit *in vacuo* and embedded in $KCrF_3$.

($PX\alpha$), indicating that the lattice effects are small and slightly increasing with R. For $R=3.93$ bohr, the distance observed in cubic $KCrF_3$, we obtain $\Delta=15.4$ (*vacuo*), 15.0 (point charges), and 14.6×10^3 cm^{-1} ($PX\alpha$). These numbers lie some 30% above the experimental range reported by Oelkrug[72] for this transition: $(10-13)\times10^3$ cm^{-1}. The value of Δ obtained at the theoretical equilibrium distance in the $PX\alpha$ calculation is $\Delta(2.112\ \text{Å})=13.3\times10^3$ cm^{-1}, in reasonable agreement with the observed range, although such agreement may be accidental.

Lattice effects obtained here for other *d-d* transitions are very similar to those shown in Fig. 8 and will not be discussed. Thus, we conclude that the cluster-lattice interaction introduces small effects in the vertical *d-d* spectrum at the *observed* R_e. This conclusion is in agreement with that discussed by Flórez *et al.*[56] for the *d-d* spectra of Mn^{2+} in octahedral fluorides, and it is related to our result that the occupied cluster MO's are slightly modified by the external lattice potential. On the other hand, the more diffuse and empty 4*s* and 4*p* MO's show larger lattice effects. We can thus expect important lattice contributions in 3*d*-4*s* and 3*d*-4*p* electronic transitions. Furthermore, the cluster-lattice interaction can produce indirect but very significant effects in transition energies, vibrational structure, and intensities, when computed at the *theoretical* R_e, due to the changes induced in the curvature of the nuclear potentials.

D. Local model-potential lattice models

We have shown the theoretical and practical advantages of a quantum-mechanical lattice model, such as the $PX\alpha$ model, over the classical description of the crystal in terms of point charges. However, since the cluster-lattice exchange interactions are substituted in the $PX\alpha$ model by the statistical approximation, we should consider the possibly unwanted consequences of this substitution in the cluster-in-the-lattice calculation. One of these consequences can be suspected from the information depicted in Fig. 5. In this figure we have seen that the exchange charge deduced from the $X\alpha$ approximation is rather long ranged and does control the lattice effective potential for $r\geq2$ bohr. This behavior would be unimportant in atomic or muffin-tin applications where the relevant contributions to the total energy and wave function are determined by the inner and central parts of the potential. In the present application, however, the slowly decreasing value of the exchange charge may produce unphysical effects on the cluster MO's. For these reasons we present now an alternative quantum-mechanical lattice model also deduced from the TES and free from the $X\alpha$ exchange approximation.

The idea of this new model is to represent the lattice ions by means of adequate local MP of the form introduced by Bonifacic and Huzinaga.[69,73,74] The difference between this scheme and the $PX\alpha$ model is the modeling of the ionic effective potentials. The use of lattice-projection operators and the further collection of the individual ionic potentials in an analytical potential is the same in both models.

In this final part we discuss some interesting systems formed by 3*d* impurities in $KMgF_3$. First, we discuss the main differences between the MP and the $PX\alpha$ lattice models. Then, we present numerical results for the equilibrium geometry of these systems, and later we refer to the question of the relative stability of different ionization states of the 3*d* impurity.

Huzinaga and his group have shown[69,73] that the electrostatic effects of the electronic core on the valence shell of an atom or ion can be accurately represented by a one-electron radial function $V_{\rm MP}(r)$ called the model potential (MP). This potential is optimized with respect to a particular atomic state and it is transferrable to other states and configurations.[74] It can also be used to study the effects of the core electrons on the valence shells of *other* atoms or ions. Here we make use of this latter application.

Since obtaining a MP is well documented in Refs. 73 and 74, we will simply list here the main steps of this procedure: (a) A given all-electron (AE) atomic calculation is chosen as reference. (b) A given basis set is selected for the valence space. It may be the basis used in the AE calculation or a smaller one. (c) Valence calculations are performed with a Fock operator in which the core-valence interactions are represented by the model potential

$$V_{\rm MP}(r)=-(Z-N_{\rm core})r^{-1}\times\left[1+\sum_{k=1}^{M}A(k)r^{n(k)}\exp[-\alpha(k)r]\right] \tag{38}$$

plus a core projector that ensures the core-valence orthogonality.

The AE solutions are used to define the core projector. The MP parameters $A(k)$, $n(k)$, and $\alpha(k)$ are chosen to minimize the error

$$\Delta=\sum_{v}^{\rm val}|\varepsilon_v^{\rm MP}-\varepsilon_v^{\rm AE}|+\sum_{v}^{\rm val}(1-|\langle\phi_v^{\rm MP}|\phi_v^{\rm AE}\rangle|)^2\ , \tag{39}$$

where the ε's are orbital energies.

In the present application, the reference state for the lattice ions must consist of a core including all the occupied orbitals of the ion because this will be the electron density seen by the cluster valence. We have chosen the $(Ar)4s^1\,^2S$ ground state of the K atom and the $(Ne)3s^1\,^2S$ ground state of the Mg^+ ion as reference states for the K^+ and Mg^{2+} ions, respectively. As AE basis sets we have used the 2-ζ set and the multi-ζ set of Ref. 70 for the K atom and the Mg^+ ion, respectively. The AE bases have also been used, without reduction, for the valence space.

To better appreciate the differences between this procedure and the $PX\alpha$ model, we present in Fig. 9 the effective charge $-rV_{\rm eff}$ for K^+ and Mg^{2+} corresponding to (a) the MP lattice model just described, (b) the $PX\alpha$ model, and (c) a Coulombic effective potential obtained through Eqs. (11) and (31) but with the exchange part neglected. We can observe that the MP charge is larger than the Coulombic charge for the Mg^{2+} ion in the range $0\leq r\leq1.5$ bohr. The same result is found for the K^+ ion

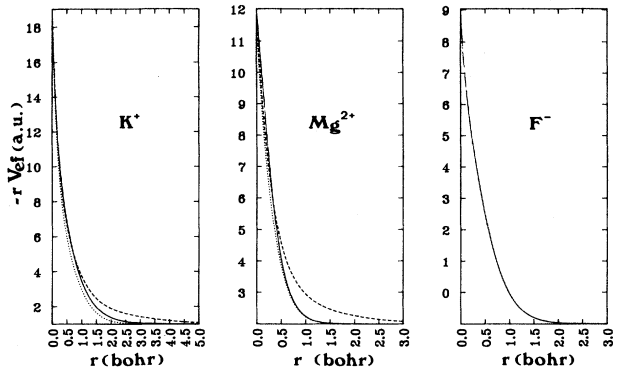

FIG. 9. Effective charge for the three ions of $KMgF_3$ obtained from the MP lattice model (solid line), the $PX\alpha$ model (dashed line), and the Coulombic model (dotted line). The effective charge for the F^- ion corresponds to the Coulombic model (see the text).

in the range $0 \leq r \leq 3.0$ bohr. Both charges reach the asymptotic limit at $r = 1.5$ bohr for the Mg^{2+} ion and at $r \cong 3.0$ bohr for the K^+ ion. However, the $PX\alpha$ charge goes to the asymptotic limit much more slowly. This behavior has a noticeable influence in the action of the lattice potential.

To complete the description of the $KMgF_3$ lattice we need the MP of the F^- ion. This would require a reference calculation in some state of the F^{2-} ion. The HF solution of its (Ne)$3s^1\,^2S$ state presents severe convergence problems (analogous to those encountered in the O^{2-} ion) and gives an extremely diffuse $3s$ orbital, with a mean radius of about 35 bohr. Since this picture can hardly be appropriate to describe the F^- ions in the lattice, we have used instead the Coulombic potential computed with the basis of the F^- ion (Ref. 14). This choice, which avoids the trouble of dealing with the F^{2-} ion, may be partly justified by the similarity observed between the MP and Coulombic potentials of the K^+ and Mg^{2+} ions (see Fig. 9). Hopefully, the cluster valence will feel negligible differences between the Coulombic and MP potentials of the F^- ion even for the first shell of fluorides. We have not studied possible basis effects on the behavior of this Coulombic potential.

Once the ionic potentials are at hand, we compute the effective lattice potential as described in Sec. II C and in the Appendix. The lattice projectors have been computed using the same basis sets,[70] number of shells, and procedures detailed in Sec. III C, since the $KMgF_3$ has the same cubic fluoroperovskite structure than the $KCrF_3$.

Let us see now the results for V, Cr, and Mn impurities in $KMgF_3$. The cluster-in-the-lattice nuclear potentials obtained with the MP lattice model for several ionization states of these ions are collected in Table III. Computed equilibrium metal-ligand distances can be seen in Fig. 10, where $R_0 = 2.005$ Å, R_V, and R_L correspond to pure $KMgF_3$ (observed), cluster-*in vacuo*, and cluster-in-the-lattice calculations, respectively.

In this figure we first notice that R_V is larger than R_0 for dipositive cations. This result agrees with the known

TABLE III. Cluster valence energy for several $3d$ impurities corresponding to cluster-*in vacuo* E_0 and cluster-in-$KMgF_3$ calculations in terms of the model-potential lattice model E_{MP}.

		$R(M\text{-}L)$								
System	Quantity	3.00	3.20	3.40	3.60	3.80	4.00	4.20	4.40	
$(VF_6)^{4-}$	E_0+208	−0.990 48	−1.526 90	−1.833 47	−1.996 72	−2.070 98	−2.089 80	−2.073 76	−2.035 55	
	$E_{MP}+208$	−4.043 54	−4.573 37	−4.873 76	−5.030 80	−5.095 28	−5.092 28	−5.025 26	−4.875 10	
$(VF_6)^{3-}$	E_0+208	−2.121 55	−2.542 80	−2.742 52	−2.810 38	−2.800 92	−2.756 68	−2.666 80	−2.572 41	
	$E_{MP}+208$	−4.405 63	−4.819 08	−5.010 96	−5.069 97	−5.046 80	−4.965 39	−4.827 87	−4.614 17	
$(MnF_6)^{4-}$	E_0+240	−1.040 76	−1.669 37	−2.024 78	−2.213 37	−2.300 02	−2.323 75	−2.308 16	−2.267 72	
	$E_{MP}+240$	−4.100 56	−4.725 16	−5.076 89	−5.261 40	−5.339 91	−5.342 97	−5.277 05	−5.124 32	
$(MnF_6)^{3-}$	E_0+240	−2.307 71	−2.723 64	−2.914 93	−2.974 08	−2.956 12	−2.893 32	−2.804 60	−2.701 14	
	$E_{MP}+240$	−4.598 23	−5.008 53	−5.193 97	−5.245 86	−5.215 25	−5.125 85	−4.979 68	−4.756 44	
		3.26	3.425	3.59	3.772	3.99	4.19	4.39	4.59	4.99
$(CrF_6)^{5-}$	E_0+222	−0.942 03	−1.347 59	−1.619 61		−1.952 79	−2.021 28	−2.053 61	−2.061 54	−2.032 18
	$E_{MP}+222$	−4.764 49	−5.170 45	−5.442 91		−5.758 86	−5.784 75	−5.714 81	−5.503 73	−4.228 29
$(CrF_6)^{4-}$	E_0+222	−2.663 89	−2.908 18	−3.049 72	−3.126 76	−3.149 17	−3.127 86	−3.081 68		
	$E_{MP}+222$	−5.718 48	−5.961 96	−6.102 42	−6.175 13	−6.179 39	−6.111 98	−5.959 73		
		3.05	3.15	3.26	3.425	3.59	3.99	4.39		
$(CrF_6)^{3-}$	E_0+222	−3.474 93	−3.664 54	−3.805 23	−3.919 07	−3.952 73	−3.853 14	−3.641 30		
	$E_{MP}+222$	−5.763 25	−5.950 94	−6.089 82	−6.201 21	−6.231 57	−6.101 18	−5.725 28		

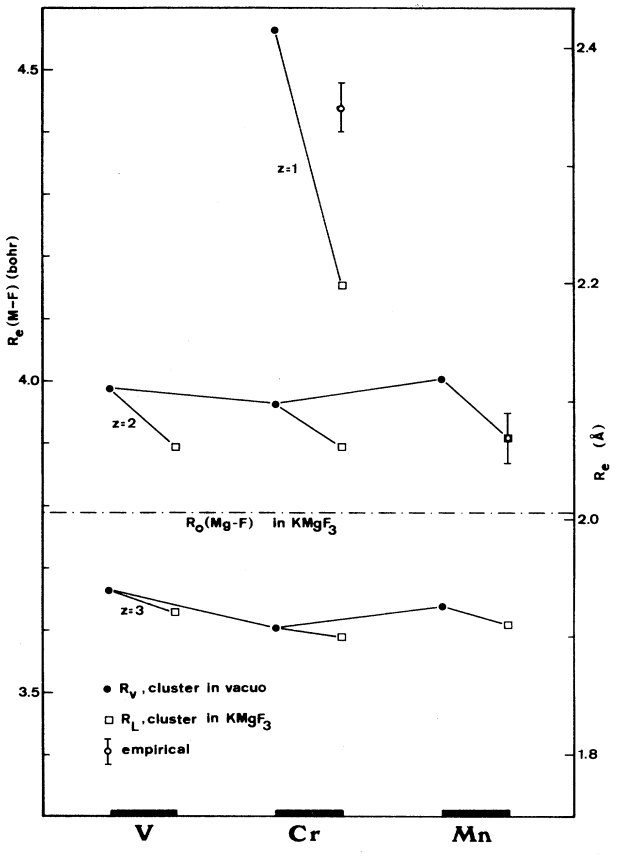

FIG. 10. Equilibrium geometry obtained from cluster-*in vacuo* and cluster-in-$KMgF_3$ calculations for several 3*d* impurities.

ionic radii[75] and suggests that the lattice effects will tend to decrease R_V. We can thus expect that $R_V > R_L$. Moreover, since the ionic radii of the 3*d* dipositive cations are larger than the radius of Mg^{2+}, the impurity substitution should induce an outwards relaxation of the first neighbors, i.e., we can also expect that $R_L > R_0$. Our theoretical results agree with both expectations. Also, our value of R_L for Mn^{2+}:$KMgF_3$ (2.070 Å) nearly coincides with those derived by Moreno *et al.*[76] from the observed superhyperfine constant A_s (2.070±0.020 Å) and $10Dq$ (2.064±0.004 Å).[77]

According to our cluster-*in vacuo* results, the ionic radius $r(Cr^+)$ can be 0.4 Å larger than $r(Mg^{2+})$. This would lead to a large outwards lattice relaxation, with $R_V > R_L > R_0$. Although both inequalitits are confirmed by our HFR results, the cluster contraction predicted in passing from *vacuo* to the lattice 0.22 Å is possibly too big. Our calculation give $R_L = 2.198$ Å, 0.15 Å below the 2.35±0.02 Å estimated semiempirically[78] from the A_s constant observed in Cr^+:$KMgF_3$. This discrepancy can be qualitatively understood in terms of the limitations of our impurity model. The Cr^+ ion is possibly too large to induce relaxations only on the first neighbors. If we include relaxations of other shells, the difference $|R_L - R_V|$ tends to decrease. However, we have not analyzed second-neighbor effects in detail and will stop the discussion of this question here.

Finally, the tripositive impurities turn out to be slightly smaller (some 0.05 Å) than the Mg^{2+} ion, according to our cluster-*in vacuo* results. Thus, we can expect inwards relaxations of the first neighbors upon this substitution. Our HFR results give $R_L < R_0$ and a very small difference (about 0.01–0.02 Å) between R_V and R_L.

To end this section, we will present some numerical examples showing that the cluster-lattice interaction plays also a substantial role in determining the relative stability of different ionization states of the 3*d* impurity in the ionic host. For a cluster as those discussed in this paper, the relative stability can be analyzed as a function of the internuclear coordinates along different cluster vibrations. We will refer here to the a_{1g} vibration of several $(MF_6)^{n-}$ clusters: M=Cr, V, and Mn; $n=2-5$. This vibration is characterized by the single metal-ligand coordinate R.

Let us discuss first the cluster-*in vacuo* description. At infinite separation ($R=\infty$), we have the free-ion energy of the M^{z+} impurity ion plus six times the free-ion energy of the F^- ion. At this configuration, our basis gives an energy for the $(M^{z+}+6F^-)$ systems that increases with increasing metallic ionization, in qualitative agreement with the observed ionization potentials (IP). For instance, the Cr^{2+} ion appears 13.64 eV above the Cr^+ ion, the Cr^{3+} 29.62 eV above the Cr^{2+}, and the Cr^{4+} 50.03 eV above the Cr^{3+}. These numbers compare well with the observed IP's of chromium:[79] 16.50 (Cr^+), 30.96 (Cr^{2+}), and 49.1 eV (Cr^{3+}). At very large values of R, the (*in vacuo*) intracluster interactions can be well represented by the classical limit

$$E[(MF_6)^{n-};\ \text{large } R]=E_{\text{class}}[(MF_6)^{n-}]$$
$$=E(R=\infty)+A/R\ , \qquad (40)$$

where the constant A is given by the point-charge interactions

$$A=6q_Mq_L+[6(2)^{1/2}+\tfrac{3}{2}]q_L^2\ . \qquad (41)$$

In Eq. (41), q_M and q_L are point charges representing the metal and fluoride ions, respectively.

The relative positions of the infinite-separation configurations hold for large values of R, although this regime clearly corresponds to unphysical cluster sizes. When R goes down to the order of a few angstroms, the pure electrostatic interaction is enough to rearrange the energy ordering of these clusters. Moreover, at small R's the nonclassical intracluster energy becomes important, modifies the energy in Eq. (40), and the minima of the nuclear potentials appear. The sum of the energy in Eq. (40) and the nonclassical contribution produces a new ordering of the cluster energies at the bonding region, as can be seen for Cr, V, and Mn hexafluorides in Figs. 11(a), 12(a), and 13(a), respectively. According to these cluster-*in vacuo* results, the state of highest ionization lies at the bottom of each series and has the smaller cluster size. As the metallic charge decreases, the size of the cluster increases and the energy at the minimum increases. In these charged and highly ionic systems the

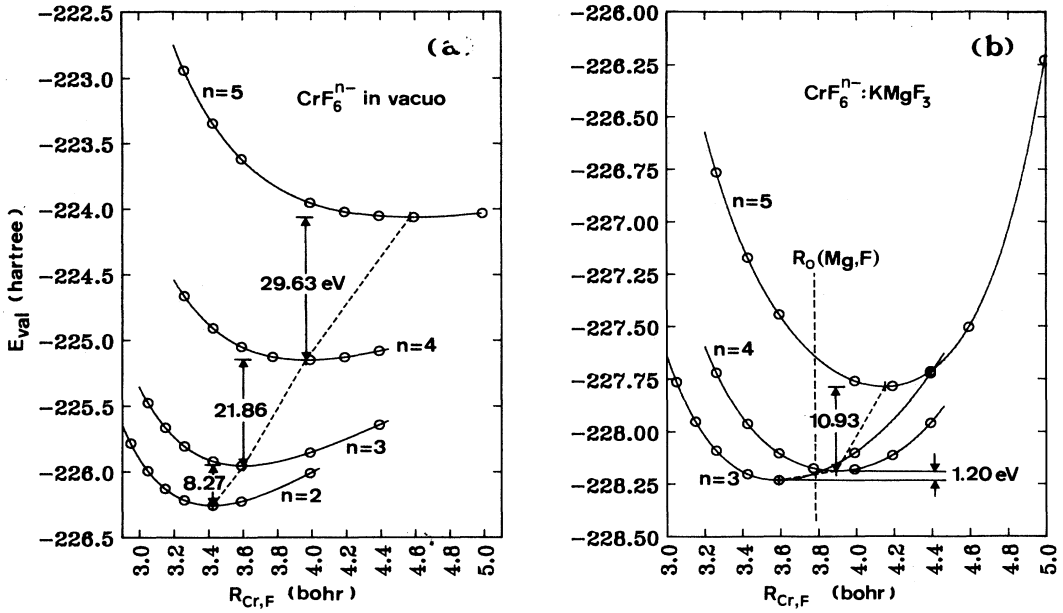

FIG. 11. Nuclear potentials for chromium impurities in fluoride crystals. (a) Cluster-*in vacuo* results. (b) Cluster-in-$KMgF_3$ results.

nonclassical contribution to the nuclear potential, albeit very important, is a small amount of the total valence energy of the cluster. In the cases considered here, the nonclassical energy is smaller than 1 hartree and the valence energy is larger than 200 hartrees. This fact suggests that the relative energy position, near R_e, of different ionization states of these impurities can be very sensitive to the action of an extracluster potential.

Our cluster-in-the lattice calculations for these impurities in $KMgF_3$ reveal that the relative stabilities of different ionization states change very much when the cluster-lattice interaction is included. These results can be seen in Figs. 11(b), 12(b), and 13(b). In Fig. 11 we observe, for instance, that the interminima energy separation for Cr^+ and Cr^{2+} is 29.63 eV *in vacuo,* but only 10.93 eV in the MP potential of $KMgF_3$. The 21.86 eV

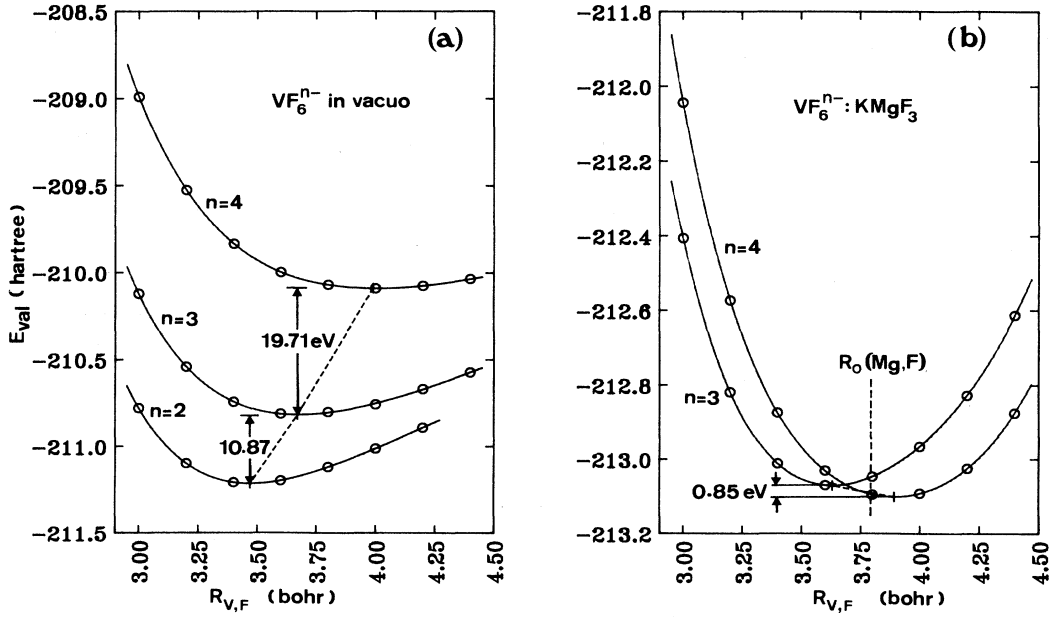

FIG. 12. Nuclear potentials for vanadium impurities in fluoride crystals. (a) Cluster-*in vacuo* results. (b) Cluster-in-$KMgF_3$ results.

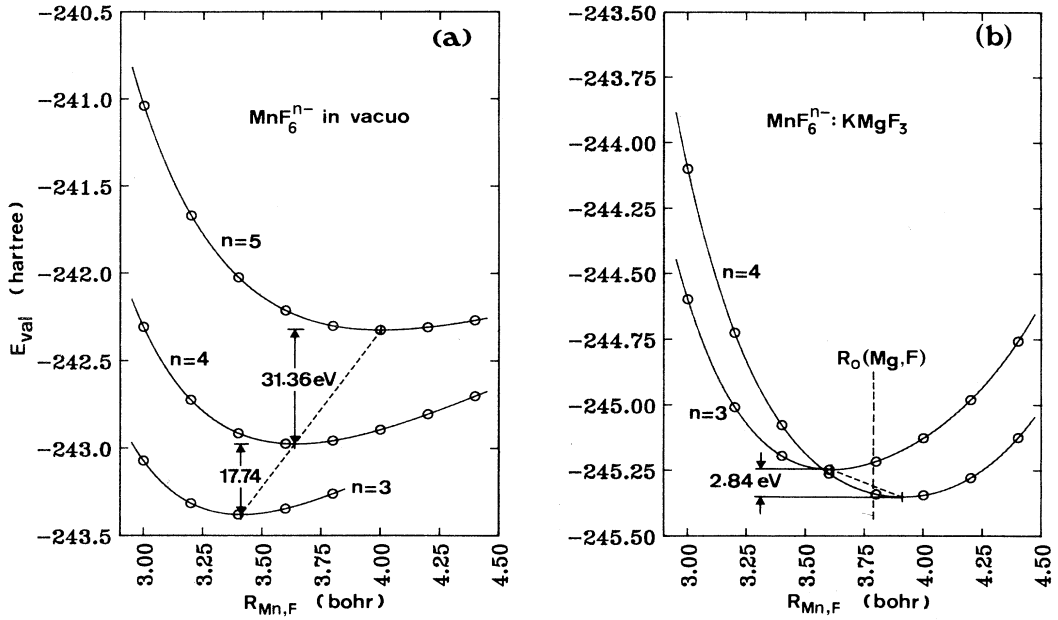

FIG. 13. Nuclear potentials for manganese impurities in fluoride crystals. (a) Cluster-*in vacuo* results. (b) Cluster-in-$KMgF_3$ results.

separating the Cr^{2+} and Cr^{3+} ions *in vacuo* are reduced to 1.20 eV in the lattice. Figure 11(b) shows that these two ions can be stable in $KMgF_3$, depending upon the metal-ligand distance. The relation between the rates of the redox process and the lattice relaxation would determine the most stable configuration. In Figs. 12 and 13 we can see that the dipositive state is more stable than the tripositive state for V and Mn in $KMgF_3$.

These numerical results have been presented here to emphasize the importance of the cluster-lattice interaction in the relative energies of different valence states of $3d$ impurities in ionic crystals. However, the present calculation gives only a crude approximation to the problem because we have considered the simple redox process

$$M^{z+}{:}\mathrm{KMgF_3} \rightleftharpoons M^{z+1}{:}\mathrm{KMgF_3} + e^- , \tag{42}$$

where the resulting electron has been considered as a zero-energy particle. The redox process to be considered should be

$$M^{z+}{:}\mathrm{crystal} \rightleftharpoons M^{z+1}{:}\mathrm{crystal} + e^-{:}\mathrm{crystal} \tag{43}$$

and adequate attention should be paid to the final state of the electron into the crystal. Such detailed description has been not attempted in this work.

IV. CONCLUSIONS

The cluster model is an important tool to compute the electronic structure of transition-metal ions in ionic lattices. However, many important properties of these systems cannot be described by a cluster-*in vacuo* approach. The cluster-lattice interaction becomes an essential part of the theoretical analysis. We have tried to show in this paper that the theory of electronic separability (TES) provides a rigorous framework to formulate the cluster model and to take adequately in account this interaction.

According to the TES, SCF cluster wave functions can be obtained which are consistent with a given electronic structure of the crystal lattice. Each ion in the lattice contributes to the cluster effective Hamiltonian with an effective potential operator, containing nuclear attraction, Coulomb and exchange interactions, and a projection operator which takes care of the cluster-lattice orthogonality requirements.

Many approximate lattice models can be developed from the basis equations of the TES, each model being characterized by the particular form of the effective potential and the wave functions selected for the lattice ions. We have discussed here three TES-consistent lattice models and illustrated their relative merits with appropriate numerical examples.

The point-charge model can be deduced from the TES by representing the lattice-ion orbitals by Dirac-δ functions, if exchange and lattice-projection terms are neglected. Neglect of these quantum-mechanical terms may give rise to important deficiencies, as we have shown for the ground-state nuclear potential of the $(CrF_6)^{4-}$ unit embedded in the vibrating lattice of $KCrF_3$.

In the $PX\alpha$ model discussed in this paper, the lattice ions are described by HFR wave functions whereas the $X\alpha$ statistical approximation is used to deal with the cluster-lattice exchange. The model contains all the terms appearing in the basic equations of the TES. In particular, the lattice-projection terms play an essential role in removing the deficiencies of the point-charge model. On the other hand, some spectral properties, like the vertical *d-d* spectrum or the orbital energies of the cluster

states, seem to be rather independent of the lattice model used.

Finally, we have examined a model-potential lattice model that describes the effective potentials of the lattice by means of an accurate local model potential. This model gives a consistent picture of cluster equilibrium geometries, vibration frequencies, relative stabilities of different ionization states, and other electronic properties of V, Cr, and Mn impurities in $KMgF_3$.

We have tried to emphasize the convenience, in a cluster calculation, of considering the cluster-lattice interaction at a level of quality commensurate with that achieved in the cluster-*in vacuo* description. The desirable balance is lacking, for instance, if a point-charge lattice is interfaced with a highly sophisticated cluster methodology. Our approximate results show that for a given cluster description the quantum-mechanical representation of the lattice may give results at substantial variance with those obtained from the point-charge model. It is our view that rigorous descriptions of the crystal lattice as those presented in this paper are thus worthwhile and workable without prohibitive effort.

Several future developments can be advanced in connection with the present TES formulation of the cluster model. First, a more rigorous treatment of the important cluster-lattice exchange interaction may be considered, as in the recent work by Barandiarán and Seijo[28,80] in which a nonlocal exchange operator is introduced within the MP formalism. Second, a description of the lattice ions more realistic than that supplied by the (*in vacuo*) HF wave functions might be attempted in order to reach an environment-consistent picture of the frozen lattice ions.[44,81] We are presently working on these developments.

ACKNOWLEDGMENTS

We want to express our thanks to M. Bermejo and J. M. Recio for many discussions on cluster models and the cluster-lattice interaction. We are also grateful to Professors R. M. Pitzer, W. C. Nieuwpoort, J. M. Vail, and L. Seijo for sending us copies of their work prior to publication. Financial support from the Dirección General de Investigación Científica y Técnica, Project No. PB86-0240 is gratefully acknowledged.

APPENDIX

We want to find an approximate analytical representation $V_{\rm fit}(r)$ for the lattice potential $V_{\rm ext}(r)$ which should be simpler than the Ewald sum in Eq. (29) and accurate enough to describe correctly the potential in those cluster regions where the electronic density is high. $V_{\rm ext}(r)$ and $V_{\rm fit}(r)$ should transform as the totally symmetric irreducible representation Γ_1 of the cluster group. This requirement is immediately satisfied if we express $V_{\rm fit}(r)$ as a linear combination of Γ_1 functions. A complete set of such functions for the O_h and T_d groups $\{f_k(x,y,z)\}$ can easily be found in terms of the even powers of the radial coordinate: $r^{2n}=(x^2+y^2+z^2)^n$, in Cartesian coordinates. See Table IV.

TABLE IV. Approximate analytical representation of the lattice potential; (upper) Γ_1 functions for cubic groups; (lower) expansion of the even powers of the radial coordinate r in terms of the Γ_1 functions.

$$
\begin{aligned}
f_0&=1\\
f_1&=x^2+y^2+z^2\\
f_2&=x^4+y^4+z^4\\
f_3&=x^2y^2+y^2z^2+z^2x^2\\
f_4&=x^6+y^6+z^6\\
f_5&=x^4y^2+x^4z^2+y^4x^2+y^4z^2+z^4x^2+z^4y^2\\
f_6&=x^2y^2z^2\\
f_7&=x^8+y^8+z^8\\
f_8&=x^6y^2+x^6z^2+y^6x^2+y^6z^2+z^6x^2+z^6y^2\\
f_9&=x^4y^4+y^4z^4+z^4x^4\\
f_{10}&=x^4y^2z^2+x^2y^4z^2+x^2y^2z^4\\
f_{11}&=x^{10}+y^{10}+z^{10}\\
f_{12}&=x^8y^2+x^8z^2+y^8x^2+y^8z^2+z^8x^2+z^8y^2\\
f_{13}&=x^6y^4+x^6z^4+y^6x^4+y^6z^4+z^6x^4+z^6y^4\\
f_{14}&=x^6y^2z^2+x^2y^6z^2+x^2y^2z^6\\
f_{15}&=x^2y^4z^4+x^4y^2z^4+x^4y^4z^2
\end{aligned}
$$

$$
\begin{aligned}
r^0&=f_0\\
r^2&=f_1\\
r^4&=f_2+2f_3\\
r^6&=f_4+3f_5+6f_6\\
r^8&=f_7+4f_8+6f_9+12f_{10}\\
r^{10}&=f_{11}+5f_{12}+10f_{13}+20f_{14}+30f_{15}
\end{aligned}
$$

We can write

$$V_{\rm fit}(r)=\sum_k c_k r^{n(k)} f_k(x,y,z)\ , \tag{A1}$$

where the c_k coefficients are obtained through least-squares minimization of the rms deviation

$$\delta=\left[N^{-1}\sum_{i=1}^{N}[V_{\rm ext}(r_i)-V_{\rm fit}(r_i)]^2\right]^{1/2}\ . \tag{A2}$$

In this equation, N is the number of points r_i where the

TABLE V. Point-charge lattice potential for the cubic phase of the $KCrF_3$ ($\mathbf{a}=4.158$ Å), Eq. (A1), and linear coefficients c_k in atomic units.

c_k	Totally symmetric function
$-0.739\,483\,96$	r^0
$-0.955\,653\,89\times10^{-4}$	r^2
$-0.557\,813\,85\times10^{-4}$	r^4
$-0.461\,600\,53\times10^{-5}$	r^6
$-0.744\,992\,54\times10^{-7}$	r^8
$-0.520\,720\,99\times10^{-4}$	r^0f_3
$-0.132\,225\,75\times10^{-4}$	r^2f_3
$-0.171\,190\,07\times10^{-4}$	r^3f_3
$-0.513\,264\,78\times10^{-3}$	r^0f_6
$-0.859\,386\,13\times10^{-6}$	r^2f_6
$-0.596\,755\,34\times10^{-5}$	r^0f_9

rms deviation = $0.280\,107\,19\times10^{-3}$

lattice potential is computed.

We would like to remark that a large number of points *throughout* the cluster volume must be considered in order to have accurate representations of the lattice potential. A set of points limited to the 100, 110, and 111 directions may give forms for $V_{\rm fit}(r)$ which reproduce poorly the features of the potential along the low-symmetry directions. These forms may give rise to qualitatively erroneous results in the cluster-in-the-lattice calculations.

When dealing with a cubic fluoroperovskite as the $KCrF_3$, the three planes passing through each two of the 100, 110, and 111 directions determine a volume element that reproduces the entire space by symmetry operations. Thus, we limit our search to points within this volume element. On the other hand, we have found that the features of the lattice potential relevant to the cluster calculations discussed in this work are those within a sphere centered in the metal ion and radius 5 bohr. Accordingly, we made the following selection of points: (a) 51 points along the 100 axis uniformly distributed within the segment (0–5 bohr); (b) 20 points uniformly distributed along every one of the 9 axes defined by the angles $\theta=90°$ and $\phi=5m°(m=1$ to 9); (c) 150 points randomly distributed within the space limited by the sphere of radius 5 bohr and the 100-110-111 volume element defined above.

The symmetry of the potential makes this set equivalent to a set of 11 586 points within the entire volume. The present choice of points weights the representation of $V_{\rm ext}(r)$ in the regions close to the xy, xz, and

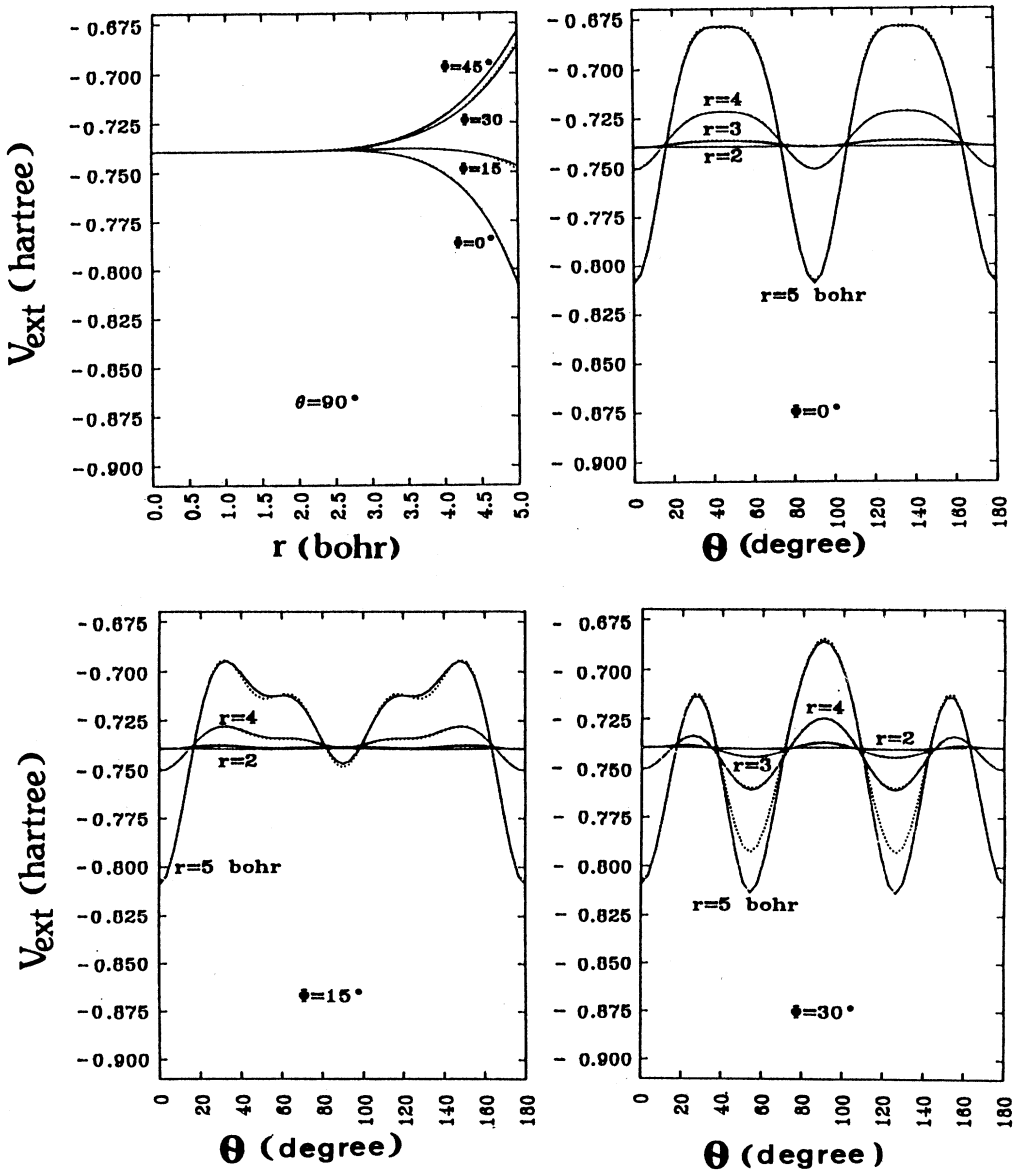

FIG. 14. Lattice potential of the cubic $KCrF_3$ crystal along several directions. Solid lines correspond to $V_{\rm ext}(r)$ and dotted lines to $V_{\rm fit}(r)$.

yz planes where the cluster electron density is higher.

In Table V we collect the final form for $V_{\text{fit}}(r)$ adopted in this work and the numerical coefficients resulting from the least-squares fitting to $V_{\text{ext}}(r)$. The rms deviation is smaller than 3×10^{-4} hartree. In Fig. 14 we plot $V_{\text{ext}}(r)$ and $V_{\text{fit}}(r)$ along several directions of interest. We can observe that $V_{\text{fit}}(r)$ reproduces uniformly well the lattice potential, with some appreciable deviations near the 111 direction and $r=4$ bohr. The interesting features of the lattice potential of this cubic fluoroperovskites along low-symmetry directions have been discussed in a recent report.[82]

[1]S. Sugano and R. G. Shulman, Phys. Rev. **130**, 517 (1963).
[2]R. E. Watson and A. J. Freeman, Phys. Rev. **134**, A1526 (1964).
[3]E. Simanek and Z. Sroubek, Phys. Status Solidi **4**, 251 (1964).
[4]S. Sugano and Y. Tanabe, J. Phys. Soc. Jpn. **20**, 1155 (1965).
[5]P. O'D. Offenhartz, J. Chem. Phys. **47**, 2951 (1967).
[6]D. E. Ellis, A. J. Freeman, and P. Ros, Phys. Rev. **176**, 688 (1968).
[7]H. M. Gladney and A. Veillard, Phys. Rev. **180**, 385 (1969).
[8]J. W. Richardson, D. M. Vaught, T. F. Soules, and R. R. Powell, J. Chem. Phys. **50**, 3633 (1969).
[9]J. W. Moskowitz, C. Hollister, and C. J. Hornback, J. Chem. Phys. **53**, 2570 (1970).
[10]T. F. Soules, J. W. Richardson, and D. M. Vaught, Phys. Rev. B **3**, 2186 (1971).
[11]J. W. Richardson, T. F. Soules, D. M. Vaught, and R. R. Powell, Phys. Rev. B **4**, 1721 (1971).
[12]A. J. H. Wachters and W. C. Nieuwpoort, Phys. Rev. B **5**, 4291 (1972).
[13]S. Larsson, E. Viinika, M. L. de Siqueira, and J. W. D. Connolly, Int. J. Quantum Chem. Symp. **8**, 145 (1974).
[14]L. Pueyo and J. W. Richardson, J. Chem. Phys. **67**, 3583 (1977).
[15]H. Adachi, S. Shiokawa, M. Tsukada, C. Satoko, and S. Sugano, J. Phys. Soc. Jpn. **47**, 1528 (1979).
[16]H. Chermette and C. Pedrini, J. Chem. Phys. **75**, 1869 (1981); **77**, 2460 (1982).
[17]C. Pedrini and H. Chermette, Int. J. Quantum Chem. **23**, 1025 (1983).
[18]E. Miyoshi, T. Takada, S. Obara, H. Kashiwagi, and K. Ohno, Int. J. Quantum Chem. **19**, 451 (1981); **23**, 1753 (1983).
[19]E. Miyoshi and H. Kashiwagi, Int. J. Quantum Chem. **24**, 85 (1984).
[20]S. Yu. Shashkin and W. A. Goddard III, Phys. Rev. B **33**, 1353 (1986).
[21]N. E. Brener and J. Callaway, Phys. Rev. B **35**, 4001 (1987).
[22]G. J. M. Janssen, Ph.D. thesis (University of Groningen, 1986) (unpublished).
[23]G. J. M. Janssen and W. C. Nieuwpoort, Phys. Rev. B **38**, 3449 (1988).
[24]G. J. M. Janssen and W. C. Nieuwpoort, Philos. Mag. B **51**, 127 (1985).
[25]N. W. Winter and R. M. Pitzer, in *Tunable Solid State Lasers,* Vol. 47 of *Springer Series in Optical Sciences,* edited by P. Hammerling (Springer, Berlin, 1985).
[26]N. W. Winter, R. M. Pitzer, and D. K. Temple, J. Chem Phys. **86**, 3549 (1987); **87**, 2945 (1987).
[27]N. W. Winter and R. M. Pitzer, J. Chem. Phys. **89**, 446 (1988).
[28]Z. Barandiarán and L. Seijo, J. Chem. Phys. **89**, 5739 (1988).
[29]A. B. Kunz, J. Meng, and J. M. Vail, Phys. Rev. B **38**, 1064 (1988).
[30]A. B. Kunz and J. M. Vail, Phys. Rev. B **38**, 1058 (1988).
[31]C. Pisani and R. Dovesi, Theor. Chim. Acta **72**, 277 (1987).
[32]V. Luaña, E. Francisco, M. Flórez, J. M. Recio, and L. Pueyo, J. Chim. Phys. (Paris) **84**, 863 (1987).
[33]R. G. Parr, F. O. Ellison, and P. G. Lykos, J. Chem. Phys. **24**, 1106 (1956).
[34]P. G. Lykos and R. G. Parr, J. Chem. Phys. **24**, 1166 (1956).
[35]J. C. Phillips and L. Kleinman, Phys. Rev. **116**, 287 (1959).
[36]L. Szász, Z. Naturforsch. **14a**, 1014 (1959).
[37]L. Szász, *Pseudopotential Theory of Atoms and Molecules* (Wiley, New York, 1985).
[38]J. D. Weeks and S. A. Rice, J. Chem. Phys. **49**, 2741 (1968).
[39]J. D. Weeks, A. Hazi, and S. A. Rice, Adv. Chem. Phys. **16**, 283 (1969).
[40]R. McWeeny, Proc. R. Soc. London, Ser. A **253**, 242 (1959).
[41]R. McWeeny and B. T. Sutcliffe, *Methods of Molecular Quantum Mechanics* (Academic, London, 1969).
[42]S. Huzinaga and A. A. Cantu, J. Chem. Phys. **55**, 5543 (1971).
[43]S. Huzinaga, D. McWilliams, and A. A. Cantu, Adv. Quantum Chem. **7**, 187 (1973).
[44]V. Luaña and L. Pueyo, J. Mol. Struct. **166**, 215 (1988).
[45]V. Luaña, G. Fernández Rodrigo, E. Francisco, L. Pueyo, and M. Bermejo, J. Solid State Chem. **66**, 263 (1987).
[46]G. Höjer and J. Chung, Int. J. Quantum Chem. **14**, 623 (1978).
[47]V. Luaña and L. Pueyo, Int. J. Quantum Chem. **31**, 975 (1987).
[48]J. Andzelm, E. Radzio-Andzelm, Z. Barandiarán, and L. Seijo, J. Chem Phys. **83**, 4565 (1985).
[49]C. C. J. Roothaan, Rev. Mod. Phys. **32**, 179 (1960).
[50]L. Seijo, Z. Barandiarán, V. Luaña, and L. Pueyo, J. Solid State Chem. **61**, 269 (1986).
[51]B. L. Kalman and J. W. Richardson, J. Chem. Phys. **55**, 4443 (1971).
[52]E. Francisco, Ph.D. thesis, Universidad de Oviedo, 1988 (unpublished).
[53]J. W. Richardson, W. C. Nieuwpoort, R. R. Powell, and W. F. Edgell, J. Chem. Phys. **36**, 1057 (1962).
[54]J. W. Richardson, R. R. Powell, and W. C. Nieuwpoort, J. Chem. Phys. **38**, 796 (1963).
[55]V. Luaña, G. Fernández Rodrigo, M. Flórez, E. Francisco, J. M. Recio, J. F. Van der Maelen, L. Pueyo, and M. Bermejo, Cryst. Lattice Defects Amorph. Mater. **15**, 19 (1987).
[56]M. Flórez, L. Seijo, and L. Pueyo, Phys. Rev. B **34**, 1200 (1986), and references quoted therein.
[57]E. Francisco, M. Flórez, Z. Barandiarán, G. Fernández Rodrigo, V. Luaña, J. M. Recio, M. Bermejo, L. Seijo, and L. Pueyo, Cryst. Lattice Defects Amorph. Mater. **15**, 45 (1987).
[58]M. Flórez, G. Fernández Rodrigo, E. Francisco, V. Luaña, J. M. Recio, J. F. Van der Maelen, L. Pueyo, M. Bermejo, M. Moreno, J. A. Aramburu, and M. T. Barriuso, Cryst. Lattice Defects Amorph. Mater. **15**, 53 (1987).
[59]M. Flórez, M. Bermejo, V. Luaña, E. Francisco, J. M. Recio, and L. Pueyo, J. Chim. Phys. (Paris) **84**, 855 (1987).
[60]E. Francisco, V. Luaña, and L. Pueyo, J. Chim. Phys. (Paris) **84**, 871 (1987).
[61]Z. Barandiarán and L. Pueyo, J. Chem. Phys. **79**, 1926 (1983).
[62]P. P. Ewald, Ann. Phys. (NY) **64**, 253 (1921).
[63]C. Kittel, *Introduction to Solid State Physics,* 2nd ed. (Wiley,

New York, 1956), Appendix A.
[64]W. Van Gool and A. G. Piken, J. Mater. Sci. **4**, 95 (1969).
[65]A. G. Piken and W. Van Gool (unpublished).
[66]J. C. Cousseins and A. DeKozak, C. R. Acad. Sci., Ser. C **263**, 1533 (1966).
[67]J. C. Slater, *The Self Consistent Field for Molecules and Solids* (McGraw-Hill, New York, 1974).
[68]S. Katsuki and M. Inokuchi, J. Phys. Soc. Jpn. **51**, 3652 (1982).
[69]V. Bonifacic and S. Huzinaga, J. Chem. Phys. **60**, 2779 (1974); **62**, 1507 (1975); **62**, 1509 (1975); **64**, 956 (1976); **65**, 2322 (1976).
[70]E. Clementi and C. Roetti, At. Data Nucl. Data Tables **14**, 177 (1974).
[71]V. Luaña, M. Bermejo, M. Flórez, J. M. Recio, and L. Pueyo, J. Chem. Phys. (to be published).
[72]D. Oelkrug, Ber. Bunsenges. Phys. Chem. **70**, 736 (1966).
[73]Y. Sakai and S. Huzinaga, J. Chem. Phys. **76**, 2537 (1982); **76**, 2552 (1982).
[74]V. Luaña, Z. Barandiarán, and L. Pueyo, J. Solid State Chem. **61**, 277 (1986)
[75]R. D. Shannon, Acta Crystallogr. Sect. A **32**, 751 (1976).
[76]M. T. Barriuso and M. Moreno, Phys. Rev. B **29**, 3623 (1984).
[77]F. Rodríguez and M. Moreno, J. Chem. Phys. **84**, 692 (1986).
[78]G. Fernández Rodrigo, L. Pueyo, M. Moreno, and M. T. Barriuso, J. Solid State Chem. **67**, 64 (1987).
[79]C. E. Moore, *Analyses of Optical Spectra,* Natl. Bur. Stand. (U.S.) Circ. No. NSRDS-NB534 (U.S. GPO, Washington, D. C., 1979).
[80]S. Huzinaga, L. Seijo, Z. Barandiarán, and M. Klobukowski, J. Chem. Phys. **86**, 2132 (1987).
[81]V. Luaña and L. Pueyo (unpublished).
[82]E. Francisco, V. Luaña, J. M. Recio, and L. Pueyo, J. Chem. Educ. **65**, 6 (1988).